经检索《**Web of Science**》和《**Journal Citation Reports（JCR）**》数据库及《中国科学院文献情报中心期刊分区表》，《**Science Citation Index Expanded (SCI-EXPANDED)**》收录论文及其期刊影响因子、中科院期刊分区信息如下。（检索时间：**2023** 年 **10** 月 **31** 日）

第 1 条，共 1 条

标题:Novel Piecewise Normalized Bistable Stochastic Resonance Strengthened Cooperative Spectrum Sensing

作者:Jiang, B(Jiang, Bin);Cao, YF(Cao, Yuefei);Bao, JR(Bao, Jianrong);Liu, C(Liu, Chao);Tang, XH(Tang, Xianghong);

来源出版物:IEEE TRANSACTIONS ON COGNITIVE COMMUNICATIONS AND NETWORKING 卷:9 期:5 页:1167-1182DOI:10.1109/TCCN.2023.3287236 出版年:OCT 2023

影响因子:8.6（2022）

中科院期刊分区:2 区（2022）

中科院 TOP 期刊:否（2022）

入藏号:WOS:001082261500005

语种:English 文献类型:Article

地址:[Jiang, Bin; Cao, Yuefei; Bao, Jianrong; Liu, Chao; Tang, Xianghong] Hangzhou Dianzi Univ, Sch Commun Engn, Hangzhou 310018, Peoples R China.

[Jiang, Bin] Hangzhou Dianzi Univ, Sch Elect & Informat, Hangzhou 310018, Peoples R China.

通讯作者地址:Bao, JR (corresponding author), Hangzhou Dianzi Univ, Sch Commun Engn, Hangzhou 310018, Peoples R China.

电子邮件地址:jiangbin@hdu.edu.cn; caoyuefei0323@163.com; baojr@hdu.edu.cn;liuchao@hdu.edu.cn; tangxh@hdu.edu.cn

ISSN:2332-7731 eISSN:

注：

中科院分区和 TOP 期刊按发表时公布的版本为准。

中科院分区依据小类就高原则。

他引次数--论文被非论文作者引用次数。

以上检索结果均得到被检索人的确认。

图书馆 信息咨询部

检索人（签章）

2023 年 10 月 31 日

Novel Piecewise Normalized Bistable Stochastic Resonance Strengthened Cooperative Spectrum Sensing

Bin Jiang, Yuefei Cao, Jianrong Bao, *Senior Member, IEEE*, Chao Liu, and Xianghong Tang

***Abstract*—A novel piecewise normalized bistable stochastic resonance (PNBSR) strengthened cooperative spectrum sensing is established by the PNBSR, residual covariance matrices, credibility weighted matrix fusion and a convolutional neural network (CNN) classification at low signal-to-noise ratios (SNRs). First, the PNBSR based on the traditional bistable stochastic resonance (TBSR) is proposed to improve the SNRs of received signals. Second, the output of the PNBSR is demodulated to obtain in-phase (I) and quadrature-phase (Q) covariance matrices. Third, the I/Q covariance matrices from different secondary users (SUs) are Cholesky decomposed to construct residual covariance matrices in a fusion center (FC). Subsequently, a new credibility weighted coefficient is proposed to fuse residual covariance matrices of the SUs. Finally, both training and test samples of the fusion detection statistics are fed into the CNN to train a high-performance classification model of cooperative spectrum sensing. The main innovations include the PNBSR, optimization index, Cholesky decomposition-based matrix cancellation to construct residual covariance matrices and credibility weighted matrix fusion. Simulation results show that the SNR of received signals strengthened by the PNBSR is improved by 3.36 dB other than received signals on average, which is 0.22dB larger than that of the TBSR. The detection probability of the proposed scheme also outperforms those of the support vector machine (SVM) and CNN schemes by 77% and 75% at −15 dB, respectively.**

***Index Terms*—Stochastic resonance, credibility weighted matrix fusion, residual covariance matrices, convolutional neural network.**

I. Introduction

AT PRESENT, with the rapid development of wireless communication technologies, two problems arose in limited spectrum resources [1], [2]. One was more spectrum resources required in wireless devices. Another was the low utilization of the authorized frequency band [3]. Spectrum sensing was one of significant techniques in cognitive radio (CR) to improve spectrum utilization [4]. Traditional spectrum sensing mainly included the energy detection (ED) [5], matched filter detection (MFD) [6], and cyclostationary feature detection (CFD) [7]. The ED had low computational complexity and no requirement for prior information of a primary user (PU). However, the performance of it was vulnerable to noise uncertainty and poor at low signal-to-noise ratios (SNRs) [8]. The MFD had advantages of short detection duration and satisfactory detection precision, but it was required for prior information of a PU [9]. Despite of satisfactory detection precision at low SNRs in the CFD, it had high computational complexity and long detection duration [10].

Given good properties of reliable communications, multiple-input multiple-output (MIMO) devices had been widely applied in spectrum sensing algorithms [11]. Most of them relied on eigenvalues of the covariance matrices [12], such as maximum and minimum eigenvalue detection (MME) [13] and variance detection among eigenvalues [14], [15]. However, only partial information in the covariance matrix was extracted to construct detection statistics. These statistics was progressive. For instance, a decision threshold was approximate and a satisfactory performance required many sample points with dramatically increased computational complexity and latency. Therefore, most MIMO algorithms had slight performance improvement compared with those of traditional ones.

To avoid the derivation of the decision threshold and problems caused by their gradualness, machine learning (ML) was introduced in spectrum sensing [16]. It was equipped with the ML technique and mainly included feature statistics construction, classification model training and testing. By this method, the decision threshold was automatically generated during the ML training. For example, spectrum sensing methods with support vector machine (SVM) were proposed in [17] and [18], in which the received signals and related signal energy were input into the SVM as a feature vector to detect PU signals. However, two major disadvantages remained as follows. First, the detection performance was strictly limited by the choice of penalty parameters and kernel functions in the SVM, and no specific rules were set on the selection of them. Second, the classification ability of the SVM was limited and only suitable for small samples training. Then, neural networks attracted more attention because of their superior performance in many

Manuscript received 15 September 2022; revised 15 January 2023 and 20 April 2023; accepted 12 June 2023. Date of publication 21 June 2023; date of current version 6 October 2023. This work was supported by the National Natural Science Foundation of China under Grant U1809201, the Fundamental Research Funds for the Provincial Universities of Zhejiang under Grant GK209907299001-003, and the Zhejiang Provincial Natural Science Foundation of China under Grant LY20F010010 and Grant LDT23F01014F01. The associate editor coordinating the review of this article and approving it for publication was Y. Zeng. *(Corresponding author: Jianrong Bao.)*

Bin Jiang is with the School of Communication Engineering and the School of Electronics and Information, Hangzhou Dianzi University, Hangzhou 310018, China (e-mail: jiangbin@hdu.edu.cn).

Yuefei Cao, Jianrong Bao, Chao Liu, and Xianghong Tang are with the School of Communication Engineering, Hangzhou Dianzi University, Hangzhou 310018, China (e-mail: caoyuefei0323@163.com; baojr@hdu.edu.cn; liuchao@hdu.edu.cn; tangxh@hdu.edu.cn).

Digital Object Identifier 10.1109/TCCN.2023.3287236

2332-7731 © 2023 IEEE. Personal use is permitted, but republication/redistribution requires IEEE permission.
See https://www.ieee.org/publications/rights/index.html for more information.

Authorized licensed use limited to: HANGZHOU DIANZI UNIVERSITY. Downloaded on October 18,2023 at 00:43:50 UTC from IEEE Xplore. Restrictions apply.

fields. In particular, the convolutional neural network (CNN) had a special network structure by extracting image features efficiently to prompt transforming spectrum sensing into image recognition. In [19] and [20], the gray image of received signals were directly fed into a CNN as characteristic statistics to train the CNN. Then, the trained CNN was used to detect PU signals with new gray images. By this method, the construction of detection statistics determined the upper limit of detection performance. The optimization by the scheme just approximated the upper limit.

The introduced ML solved the decision threshold setting, but it did not improve the detection accuracy at low SNRs. One signal improvement was proposed to make the detection statistics under different assumptions more distinguishable. The energy detection methods in [21] and [22] used stochastic resonance (SR) to improve the SNRs of received signals for better detection. The SR was firstly proposed by Benzi et al. in 1981 to investigate the Earth's palaeo-meteorological glaciers [23]. It was a nonlinear phenomenon by using noises to enhance the detection of weak signals. Initially, it only performed well in weak signal processing with frequencies and amplitudes far less than 1. To better utilize the SR in communications, scale transformation was used in the SR to enhance large-parameter signals [24]. With the deepening of the SR theory and application of the traditional bistable stochastic resonance (TBSR), the latter has suffered from the problem of easily saturated output [25] and the potential well barrier was rather high [26]. For these problems, the transform of the potential model was very helpful in improving the performance of the SR. In [27], a linear SR model was proposed to solve the above problems. However, the consistent slope of the potential well wall easily caused the output of the SR to produce more serious distortion by the noises.

Another solution to improve the detection performance at low SNRs was the cooperation among secondary users (SUs) in cognitive radio networks (CRNs). The cooperation is divided into the hard decision fusion (HDF) and soft fusion according to data types. In the HDF, only the decisions of the participating SUs were shared and the collected data in case of soft fusion was shared in the fusion center [28]. The HDF mainly included the AND, OR, K rules and the linear quadratic combining rule. In [29], the optimal decision threshold was investigated for the HDF. Although the HDF improved the detection accuracy slightly at low SNRs, it still needed to set the decision threshold K artificially regardless of the different SNR environments of the SUs. For the soft fusion, there was actually no unified and effective strategy at present.

According to current flaws of the aforementioned spectrum sensing methods, especially the poor recognition rate and the imprecise decision threshold at low SNRs, an efficient cooperative spectrum sensing is proposed by a CNN and piecewise normalized bistable stochastic resonance (PNBSR) strengthened residual covariance matrices. Besides, the main contributions of the proposed scheme are summarized concisely as follows.

- *Piecewise normalized bistable stochastic resonance-based signal enhancement to improve the SNR of the received signals:* To further improve the performance of the SR, a PNBSR system is proposed to solve the output saturation and high potential well barrier in the TBSR. Compared with the TBSR, the proposed PNBSR has a lower potential well barrier and flatter potential well wall. Thus, it easily transfers the noise energy to the useful signal one for better performance enhancement.
- *New optimization index ψ by the covariance matrix to solve the optimal PNBSR parameter a:* The system parameter a is the key for the PNBSR to generate the SR phenomenon. To optimize the parameter a efficiently, a new optimization index ψ by the covariance matrix replaces the traditional optimization index SNR_{out}, *i.e.,* the SNR of the SR output. Without prior information, the PU signals cannot be separated from noises and thus SNR_{out} is hard to be calculated. For ψ, it has the same variation trend as the SNR. SNR_{out} reaches the maximum, as well as ψ do simultaneously. But ψ requires little computation and no prior information during the optimization of the system parameter a.
- *Matrix cancellation with Cholesky decomposition to reduce the noise interference for better detection:* At low SNRs, the influence of PU signals is negligible compared with that of the noises on the covariance matrices. Therefore, for the CNN processing, the changes in the covariance matrix with or without PU signals are easily falsely judged by the randomness of noises, thereby causing the CNN unable to make correct decisions at low SNRs. Before feeding the covariance matrix into the CNN, a matrix cancellation by Cholesky decomposition is adopted to reduce the noise interference. Therefore, the influence of PU signals on the covariance matrix is enhanced to improve significantly the detection performance.
- *Efficient multiuser cooperation, called credibility weighted matrix fusion, to improve the detection accuracy of the SUs in cognitive radio networks:* A new multiuser cooperation, called credibility weighted matrix fusion, is proposed to improve the detection performance by both reducing the gradualness of the statistical covariance matrices and improving the average SNR of the SUs with credibility weights. Traditional cooperations mainly adopt the voting criterion with the minority obeying the majority to reduce the detection error probability caused by the outburst communication deterioration. However, they only provide a small performance boost and it is unfair to the SUs under different SNRs. The proposed cooperation considers the SNR in each SU and it then adopts a credibility weighted coefficient to achieve both more fairness and better performance.

The remainder of this paper is organized as follows. Section II introduces a system model of spectrum sensing in CR networks. Section III presents a new cooperative spectrum sensing algorithm. The computational complexity of the proposed and some other schemes are analyzed and compared. Section IV provides simulation results and experimental analyses to validate the good performance of the proposed spectrum sensing. Finally, Section V summarizes the whole paper.

Authorized licensed use limited to: HANGZHOU DIANZI UNIVERSITY. Downloaded on October 18,2023 at 00:43:50 UTC from IEEE Xplore. Restrictions apply.

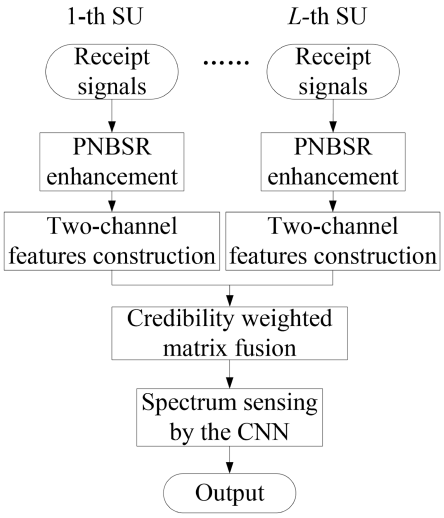

Fig. 1. Proposed cooperative spectrum sensing model.

II. System Model of Spectrum Sensing in Cognitive Radio Networks

Suppose that L SUs with M antennas are configured in a CRN and a PU is located within the detection range of the SUs [30]. The spectrum sensing is modeled as a binary hypothesis under the Neyman-Pearson and Bayes tests and it is expressed as

$$y_{i,j}(n) = \begin{cases} v_{i,j}(n) & \mathrm{H}_0 \\ s(n)h_{i,j}(n) + v_{i,j}(n) & \mathrm{H}_1, \end{cases} \tag{1}$$

where $y_{i,j}(n)$, $v_{i,j}(n)$ and $h_{i,j}(n)$ $(i = 1, 2, \ldots, L,\ j = 1, 2, \ldots, M,\ n = 1, 2, \ldots, N)$ represent received signals, additive white Gaussian noise (AWGN) with zero mean and a variance of σ_n^2, and channel gain at the *j*-th antenna and *n*-th sample in the *i*-th SU, respectively. L is the total number of the SUs. M is the total number of antennas in a SU. N is the number of sampling points in one observation obtained in a sensing slot. $s(n)$ ndicates a PU signal received by a SU. Hypotheses H_0 and H_1, respectively, denote the hypotheses of the presence or absence of a PU. The signals received by the *i*-th SU is represented as

$$\begin{aligned} \boldsymbol{Y}_i(n) &= \left[y_{i,1}(n), y_{i,2}(n), \ldots, y_{i,M}(n)\right]^T \\ &= \begin{bmatrix} y_{i,1}(1) & y_{i,1}(2) & \cdots & y_{i,1}(N) \\ y_{i,2}(1) & y_{i,2}(2) & \cdots & y_{i,2}(N) \\ \vdots & \vdots & \vdots & \vdots \\ y_{i,M}(1) & y_{i,M}(2) & \cdots & y_{i,M}(N) \end{bmatrix}. \end{aligned} \tag{2}$$

The main procedures of the cooperative spectrum sensing are designed and shown in Fig. 1 and it is divided as follows. The adjacent SUs with multiple antennas receive signals from the same PU. The received signals are fed into the piecewise normalized bistable stochastic resonance (PNBSR) to improve the SNRs. Then two-channel features are extracted with the matrix cancellation by the Cholesky decomposition. In a fusion center (FC), the proposed credibility weighted matrix fusion processes the two-channel features from different SUs to obtain the fused features. Finally, the trained CNN detects the presence or absence of PU according to the fused features.

The detection performance of spectrum sensing is mainly evaluated by the following three indicators, namely, the detection probability (P_d), false alarm probability (P_f), and missed alarm probability (P_m), respectively. They are denoted as

$$\begin{cases} P_d = P(D_1|\mathrm{H}_1) \\ P_f = P(D_1|\mathrm{H}_0) \\ P_m = P(D_0|\mathrm{H}_1) \end{cases}, \tag{3}$$

where D_1 and D_0 denote the hypotheses of the presence and absence of a PU, respectively, and it is determined by a SU detector. The definitions of the aforementioned three items are listed as follows.

P_d: when a PU is present, the SU determines the probability of its presence.

P_f: when a PU is absent, the SU determines the probability of its presence.

P_m: when a PU is present, the SU determines the probability of its absence.

III. Cooperative Spectrum Sensing With CNN and Residual Covariance Matrices Strengthened by the PNBSR

In this section, an efficient cooperative spectrum sensing with residual covariance matrices strengthened by the PNBSR, credibility weighted matrix fusion, and CNN is proposed. It mainly includes the PNBSR to improve the SNR of received signals, the credibility weighted matrix fusion for residual covariance matrices, and the CNN classification. Finally, the complexity analysis of the whole scheme is presented.

A. Cooperative Spectrum Sensing With Enhanced Residual Covariance Matrices

QPSK signals are widely used for excellent anti-noise characteristics and frequency band utilization. Thus, a PU signal with QPSK modulation is expressed as

$$\begin{aligned} s(t) &= \tilde{I}\cos(wt) - \tilde{Q}\sin(wt) \\ &= A\cos(wt + \theta), \end{aligned} \tag{4}$$

where $cos(wt)$ and $sin(wt)$ are carriers. w and θ represent carrier frequency and phase, respectively. $\tilde{I}$ and $\tilde{Q}$, respectively, are messages carried by the In-phase (I) and quadrature (Q) orthogonal signals. Then, a SU digital receiver converts the continuous domain signal $s(t)$ to a discrete sequence $s(n)$ under a sampling rate f_s. Finally, $s(n)$ is expressed as

$$\begin{aligned} s(n) &= \tilde{I}\cos(wn/f_s) - \tilde{Q}\sin(wn/f_s) \\ &= A\cos(wn/f_s + \theta). \end{aligned} \tag{5}$$

Given a received signal matrix of the *i*-th SU, *i.e.*, $\boldsymbol{Y}_i(n) = [y_{i,1}(n), y_{i,2}(n), \ldots, y_{i,M}(n)]^T$ containing M signals according to (1) and (2), the dimension of each signal is N. Then, the matrix is fed into a nonlinear system, and it is expressed with Langevin equation as

$$\frac{dx}{dt} = -\frac{dU(x)}{dx} + s(t) + v(t), \tag{6}$$

Authorized licensed use limited to: HANGZHOU DIANZI UNIVERSITY. Downloaded on October 18,2023 at 00:43:50 UTC from IEEE Xplore. Restrictions apply.

where x is the output of the nonlinear system. $s(t)$ and $v(t)$ are the PU signal and noise, respectively. $U(x)$ indicates the potential function of the SR system. Different nonlinear potential functions represent different nonlinear systems, and they can be expanded into polynomial functions by using the Taylor series expansion as

$$U(x) = a_0 + a_1 x + a_2 x^2 + a_3 x^3 + \cdots . \tag{7}$$

The potential function of the TBSR is then expressed as

$$U_{TBSR}(x) = -\frac{a}{2}x^2 + \frac{b}{4}x^4, \tag{8}$$

where a and b are nonzero system parameters. There are two steady states $x = \pm\sqrt{a/b}$ and one unstable state $x = 0$. The height difference between the steady state and the unstable state is calculated by

$$\Delta U_{TBSR} = \frac{a^2}{4b}. \tag{9}$$

In additional, the Kramers rate (r_k) is also a crucial index for the SR. In [27], r_k is defined as the rate at which a transition occurs between the steady states of the potential function. It reflects the ability of the output signals to follow noisy input signals. When the nonlinear system is only affected by noises, the Brownian particles switch between the steady states according to r_k in the potential wells. r_k is numerically the reciprocal of the mean first passage time and it is defined as

$$r_k = \mu\frac{\omega_A}{2\pi}\exp\left(-\frac{\Delta U}{D}\right) \; with \; \mu = \sqrt{U''(0) + U'''(0)}, \tag{10}$$

where μ is the correction factor and ω_A is the vibrational angular frequency of the Brownian particle at steady states. $U''(0)$ and $U'''(0)$ are the second- and third-order derivatives of $U(x)$ under $x = 0$, respectively. And r_k in the TBSR is then represented as

$$r_{TBSR} = \frac{a}{\sqrt{2}\pi}\exp\left(-\frac{a^2}{4bD}\right), \tag{11}$$

$$D = \frac{\sigma_n^2}{2}. \tag{12}$$

The large well barrier ΔU and steep well wall reduce the Kramers rate and cause the saturation to cut the enhancement of the SR system [27]. To solve them, the coefficients in the polynomial (7) are re-optimized to find a suitable potential function. Suppose that the highest degree of $U(x)$ is 4, since the derivative of a constant is 0 and the derivative of a linear term is constant. So, it is equivalent to a constant force, and thus their effects are not considered. Therefore, the optimization objective polynomial is expressed as

$$U(x) = a_2 x^2 + a_3 x^3 + a_4 x^4. \tag{13}$$

Since the term of the third degree has the property of lowering the potential well barrier and smoothing the potential well wall, the parameter a_2 is optimized by fixing a_3 and a_4, and then a new potential function is constructed. The final optimization results are shown in Fig. 2.

In Fig. 2, SNR_{out} exhibits an approximately symmetric behavior with respect to the parameter a_2, and the maximum

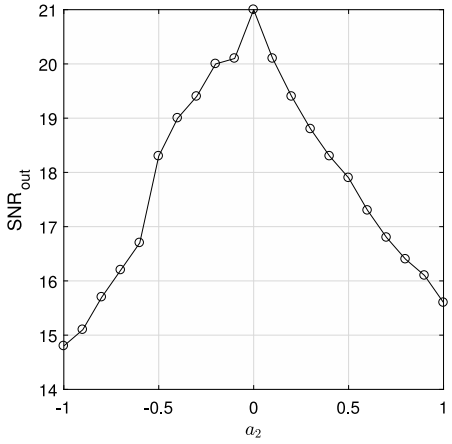

Fig. 2. SNR_{out} of $U(x)$ with different parameter a_2.

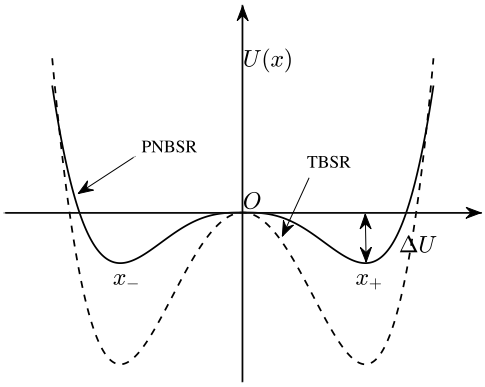

Fig. 3. The potential function of the bistable system.

SNR_{out} is achieved given $a_2 = 0$. Therefore, the term of the third degree in (13) can be set to 0 without affecting the enhancement of $U(x)$ on input signals. Hence, a piecewise normalized bistable stochastic resonance with the TBSR is generated. The piecewise potential function is expressed as

$$U_{PNBSR}(x) = \begin{cases} -\frac{a}{3}x^3 + \frac{b}{4}x^4 & x \geq 0 \\ \frac{a}{3}x^3 + \frac{b}{4}x^4 & x < 0. \end{cases} \tag{14}$$

where the term "piecewise" in the PNBSR indicates the potential function as a piecewise function. Given that the traditional SR system is only used in strengthening weak signals, like signals with a frequency and amplitude far less than 1 Hz, the SR system must be normalized for large-parameter signals.

There are two steady states $x = \pm a/b$ and one unstable state $x = 0$. The height of the well barrier of the PNBSR is calculated by

$$\Delta U_{PNBSR} = \frac{a^4}{12b^3}. \tag{15}$$

In Fig. 3, when $a = b$, the potential well barrier of the PNBSR is lower and the potential well wall is flatter than those in the TBSR. According to (10), the Kramers rate of the PNBSR is expressed as

$$r_{PNBSR} = \frac{a\sqrt{a}}{\sqrt{2b}\pi}\exp\left(-\frac{a^4}{12b^3 D}\right). \tag{16}$$

Authorized licensed use limited to: HANGZHOU DIANZI UNIVERSITY. Downloaded on October 18,2023 at 00:43:50 UTC from IEEE Xplore. Restrictions apply.

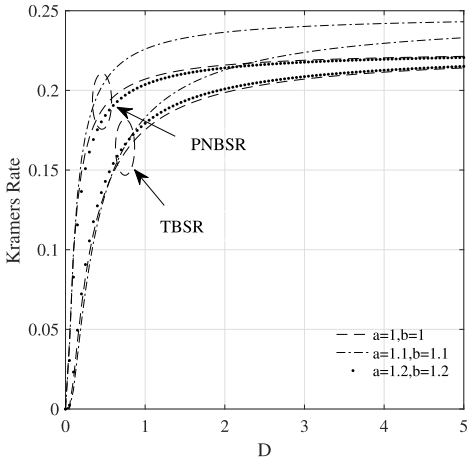

Fig. 4. The Kramers rate r_k of the PNBSR and TBSR versus D for different system parameters.

To further compare r_k in the PNBSR and TBSR, the relationships between r_k and noise intensity are plotted with three sets of system parameters in Fig. 4. Given $a = b$, r_k of the PNBSR is larger than that of the TBSR, and thus the PNBSR has a stronger ability to follow the input data.

Given that the traditional SR system is only used in strengthening weak signals, *e.g.,* signals with a frequency and amplitude far less than 1 Hz, the SR system must be normalized for large-parameter signals. Then (6) can be normalized as

$$z = x\frac{b}{a}, \tag{17}$$

$$\tau = \frac{a^2}{b}t. \tag{18}$$

By substituting (17) and (18) into (6), the PNBSR system is given as

$$\frac{a^3}{b^2}\frac{dz}{d\tau} = \pm\frac{a^3}{b^2}z^2 - \frac{a^3}{b^2}z^3 + s\left(\frac{b\tau}{a^2}\right) + v\left(\frac{b\tau}{a^2}\right). \tag{19}$$

The normalization is equivalent to a second sampling. For $s(t)$, the frequency is reduced to b/a^2. For AWGN, the independence of random variables allows noises to be viewed as

$$v\left(\frac{b\tau}{a^2}\right) = v(\tau). \tag{20}$$

Thus, the final PNBSR system is given as

$$\frac{dz}{d\tau} = \pm z^2 - z^3 + \frac{b^2}{a^3}s\left(\frac{b\tau}{a^2}\right) + \frac{b^2}{a^3}v(\tau), \tag{21}$$

where a and b are the key parameters to generate the SR. The details of optimizing a and b are discussed later. Suppose that the current SR system matches $\boldsymbol{Y}_i(n)$. Given $\boldsymbol{Y}_i(n)$, the SR system outputs $\boldsymbol{Y}_{i\_SR}(n)$ and it is represented as

$$\boldsymbol{Y}_{i\_SR}(n) = \big[s_{SR}(n)h_{i,1}(n) + v_{i,1\_SR}(n), \ldots, s_{SR}(n)h_{i,M}(n) + v_{i,M\_SR}(n)\big]^T. \tag{22}$$

Fig. 5 shows the input and output of the PNBSR. Subplots 5(a) and 5(b) are the time domain waveform and spectrum of received signal. Subplots 5(c) and 5(d) are the time domain waveform and spectrum of the output signals. The signal amplitudes presented in Fig. 5 are results of normalization amplitudes rather than the actual ones of signals. According to (21), although the amplitudes of received signals are reduced after the PNBSR compared with those without the PNBSR processing, the amplitudes of the PU signals and noises are reduced by the same factor. In addition, the PNBSR significantly reduces noises, especially the parts of high frequency. In the frequency domain, the SNR is calculated by taking the square of the amplitude of the frequency containing the PU signals. And they are divided by the sum of the squares of the noise amplitude over the entire frequency range. Therefore, the SNR is independent of the amplitudes. Under reduced high-frequency noises, the SNRs of the output signals of the PNBSR increases dramatically, thereby improving the qualities of received signals.

In [31], existing researches indicate that the difference between $s(n)$ and $s_{SR}(n)$ is the amplitude. Subsequently, it is regarded as

$$s_{SR}(n) = \frac{1}{\lambda}s(n)(\lambda > 1). \tag{23}$$

Due to the features of I /Q signals of $s_{SR}(n)$, the CNN can totally discriminate all feature differences under hypotheses H_0 and H_1 by using the I and Q components of $s_{SR}(n)$ from orthogonal demodulation. Then, the I/Q signals of $\boldsymbol{Y}_{i\_SR}(n)$ are calculated respectively as

$$\boldsymbol{I}_i(n) = \boldsymbol{Y}_{i\_SR}(n)\cos(\omega n/f_s), \tag{24}$$

$$\boldsymbol{Q}_i(n) = \boldsymbol{Y}_{i\_SR}(n)\sin(\omega n/f_s). \tag{25}$$

In traditional orthogonal demodulation, a low-pass filter is required to filter out signals other than the low frequency to extract the information carried by QPSK signals. However, given that extracting information is unnecessary in spectrum sensing, the proposed algorithm does not require a filter. The hardware complexity can thus be reduced. Then, covariance matrices of $\boldsymbol{I}_i$ and $\boldsymbol{Q}_i$ are computed as

$$E\Big[\boldsymbol{Y}\boldsymbol{Y}^H\Big] = E\Big[\boldsymbol{S}\boldsymbol{S}^H\Big] + E\Big[\boldsymbol{V}\boldsymbol{V}^H\Big] = \boldsymbol{R}_{\boldsymbol{S}} + \boldsymbol{R}_{\boldsymbol{V}}, \tag{26}$$

where $\boldsymbol{Y}$, $\boldsymbol{S}$, and $\boldsymbol{V}$ represent matrices of received signals, PU signals, and noises, respectively. $\boldsymbol{R}_{\boldsymbol{S}}$ and $\boldsymbol{R}_{\boldsymbol{V}}$ are covariance matrices of $\boldsymbol{S}$ and $\boldsymbol{V}$. Thus, covariance matrices of $\boldsymbol{I}_i$ and $\boldsymbol{Q}_i$ are denoted as

$$\begin{aligned}\boldsymbol{R}_{i\_I} &= E\Big[\boldsymbol{I}_i\boldsymbol{I}_i^H\Big] = E\Big[(\boldsymbol{S}_{\boldsymbol{i\_SR}} + \boldsymbol{V}_{\boldsymbol{i\_SR}})^2\cos^2(\omega n/f_s)\Big] \\ &= E\Big[\boldsymbol{S}_{i\_SR}{}^2\cos^2(\omega n/f_s)\Big] + E\Big[\boldsymbol{V}_{i\_SR}^2\cos^2(\omega n/f_s)\Big] \\ &\quad + 2E\Big[\boldsymbol{S}_{i\_SR}\boldsymbol{V}_{i\_SR}\cos^2(\omega n/f_s)\Big], \end{aligned} \tag{27}$$

$$\begin{aligned}\boldsymbol{R}_{i\_Q} &= E\Big[\boldsymbol{Q}_i\boldsymbol{Q}_i^H\Big] = E\Big[(\boldsymbol{S}_{i\_SR} + \boldsymbol{V}_{i\_SR})^2\sin^2(\omega n/f_s)\Big] \\ &= E\Big[\boldsymbol{S}_{i\_SR}{}^2\sin^2(\omega n/f_s)\Big] + E\Big[\boldsymbol{V}_{i\_SR}{}^2\sin^2(\omega n/f_s)\Big] \\ &\quad + 2E\Big[\boldsymbol{S}_{i\_SR}\boldsymbol{V}_{i\_SR}\sin^2(\omega n/f_s)\Big], \end{aligned} \tag{28}$$

where $\boldsymbol{S}_{i\_SR}$ and $\boldsymbol{V}_{i\_SR}$ are the SR output of $\boldsymbol{S}_i$ and $\boldsymbol{V}_i$. Due to the independence among deterministic signals

Authorized licensed use limited to: HANGZHOU DIANZI UNIVERSITY. Downloaded on October 18,2023 at 00:43:50 UTC from IEEE Xplore. Restrictions apply.

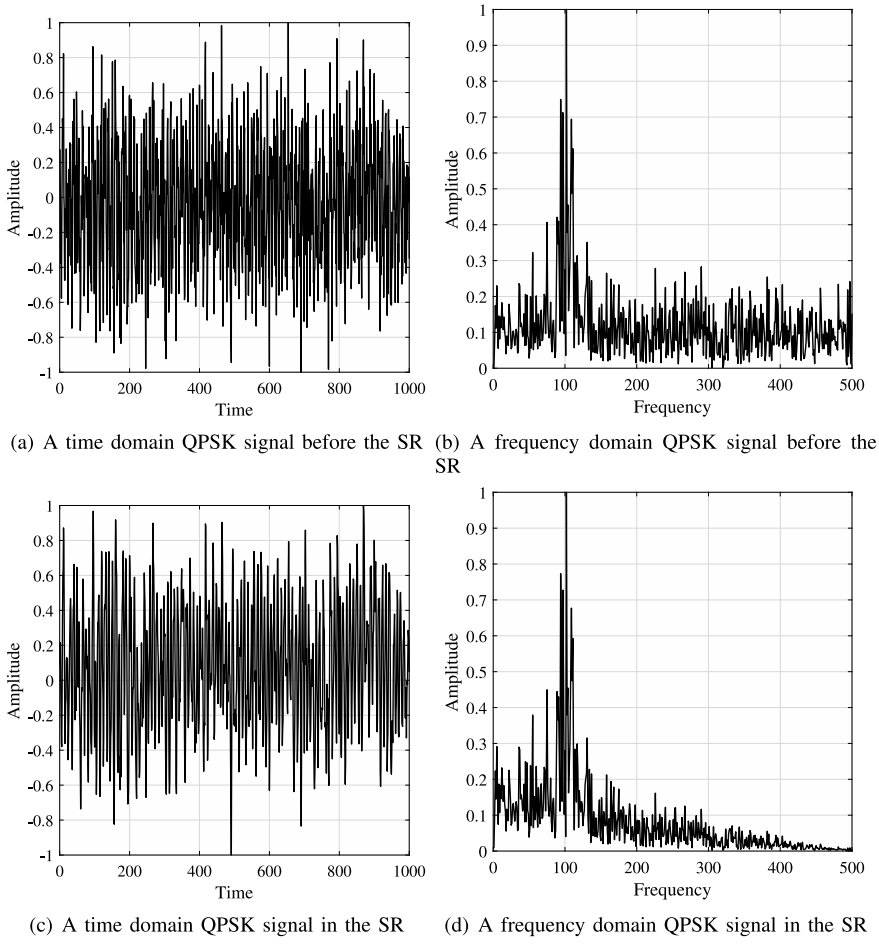

(a) A time domain QPSK signal before the SR (b) A frequency domain QPSK signal before the SR

(c) A time domain QPSK signal in the SR (d) A frequency domain QPSK signal in the SR

Fig. 5. The input and output of the PNBSR system.

and noises, the covariance matrices of $\boldsymbol{I}_i$ and $\boldsymbol{Q}_i$ are transformed to

$$\begin{aligned}\boldsymbol{R}_{i\_I} &= \boldsymbol{R}_{\boldsymbol{S}_{i\_I\_SR}} + 2E\Big[\boldsymbol{S}_{i\_SR}\cos^2(\omega n/f_s)\Big]E[\boldsymbol{V}_{i\_SR}] \\ &\quad + E\Big[\cos^2(\omega n/f_s)\Big]E\Big[\boldsymbol{V}_{i\_SR}{}^2\Big] \\ \boldsymbol{R}_{\boldsymbol{S}_{i\_I\_SR}} &= E\Big[\boldsymbol{S}_{i\_SR}{}^2\cos^2(\omega n/f_s)\Big], \qquad (29) \\ \boldsymbol{R}_{i\_Q} &= \boldsymbol{R}_{\boldsymbol{S}_{i\_Q\_SR}} + 2E\Big[\boldsymbol{S}_{i\_SR}\sin^2(\omega n/f_s)\Big]E[\boldsymbol{V}_{i\_SR}] \\ &\quad + E\Big[\sin^2(\omega n/f_s)\Big]E\Big[\boldsymbol{V}_{i\_SR}{}^2\Big] \\ \boldsymbol{R}_{\boldsymbol{S}_{i\_Q\_SR}} &= E\Big[\boldsymbol{S}_{i\_SR}{}^2\sin^2(\omega n/f_s)\Big]. \qquad (30)\end{aligned}$$

In [31], when the AWGN with zero mean and variance σ_n^2 passed through the SR system, the probability density function of the output signals can be approximately expressed as

$$p(x) = 2\left(\int_{x_-}^{x_+} e^{-\frac{a^2}{Db}U(x)}\,dx\right)^{-1} \times 2e^{-\frac{a^2}{Db}U(x)}. \qquad (31)$$

Given that $p(x)$ is symmetric, its mean and variance are calculated respectively by

$$\begin{aligned}E[X] &= \int_{-\infty}^{+\infty} xp(x)\,dx = 0, \qquad (32) \\ E\Big[X^2 - E^2[X]\Big] &= E\Big[X^2\Big] \\ &= \int_{-\infty}^{+\infty} x^2 p(x)\,dx, \\ &= \xi_n^2 \qquad (33)\end{aligned}$$

where ξ_n^2 is a variable only related to σ_n^2. Then, (28) and (29) turn into

$$\boldsymbol{R}_{i\_I} = \boldsymbol{R}_{\boldsymbol{S}_{i\_I\_SR}} + \xi_{i\_n}^2 E\Big[\cos^2(\omega n/f_s)\Big]\boldsymbol{I}_{M\times M}, \quad (34)$$

$$\boldsymbol{R}_{i\_Q} = \boldsymbol{R}_{\boldsymbol{S}_{i\_Q\_SR}} + \xi_{i\_n}^2 E\Big[\sin^2(\omega n/f_s)\Big]\boldsymbol{I}_{M\times M}. \quad (35)$$

Under different hypotheses, the statistical covariance matrices of the I/Q signals are represented as

$$\left.\begin{aligned}\boldsymbol{I} &: \xi_{i\_n}^2 E\big[\cos^2(\omega n/f_s)\big]\boldsymbol{I}_{M\times M} \\ \boldsymbol{Q} &: \xi_{i\_n}^2 E\big[\sin^2(\omega n/f_s)\big]\boldsymbol{I}_{M\times M}\end{aligned}\right\} H_0$$

$$\left.\begin{aligned}\boldsymbol{I} &: \boldsymbol{R}_{\boldsymbol{S}_{i\_I\_SR}} + \xi_{i\_n}^2 E\big[\cos^2(\omega n/f_s)\big]\boldsymbol{I}_{M\times M} \\ \boldsymbol{Q} &: \boldsymbol{R}_{\boldsymbol{S}_{i\_Q\_SR}} + \xi_{i\_n}^2 E\big[\sin^2(\omega n/f_s)\big]\boldsymbol{I}_{M\times M}\end{aligned}\right\} H_1. \quad (36)$$

In practice, the statistical covariance matrices are only estimated by the sample covariance matrices and they are defined as

$$\begin{aligned}\boldsymbol{R}_{i\_I} &\approx \tilde{\boldsymbol{R}}_{i\_I} = \frac{1}{N}\boldsymbol{I}_i\boldsymbol{I}_i^H \\ \boldsymbol{R}_{i\_Q} &\approx \tilde{\boldsymbol{R}}_{i\_Q} = \frac{1}{N}\boldsymbol{Q}_i\boldsymbol{Q}_i^H, \qquad (37)\end{aligned}$$

Authorized licensed use limited to: HANGZHOU DIANZI UNIVERSITY. Downloaded on October 18,2023 at 00:43:50 UTC from IEEE Xplore. Restrictions apply.

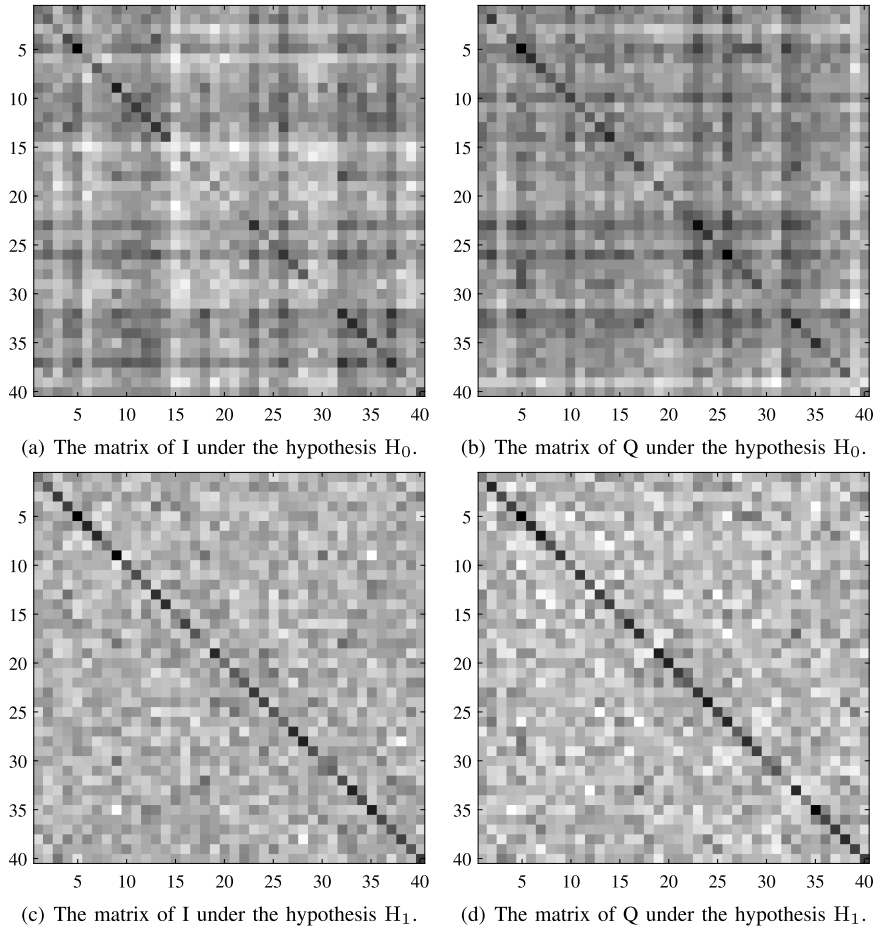

(a) The matrix of I under the hypothesis H_0. (b) The matrix of Q under the hypothesis H_0.

(c) The matrix of I under the hypothesis H_1. (d) The matrix of Q under the hypothesis H_1.

Fig. 6. Residual covariance matrices of I and Q phase signals under hypotheses H_0 and H_1.

where $\boldsymbol{R}$ and $\tilde{\boldsymbol{R}}$ indicate the statistical covariance matrix and sample covariance matrix, respectively.

There are usually several SUs in a CRN. Therefore, a new cooperation, called credibility weighted matrix fusion, is employed to improve the detection accuracy. Assume that there are L SUs for cooperative spectrum sensing. For credibility weighted matrix fusion, each SU sends their $\tilde{\boldsymbol{R}}_{i\_I}$ and $\tilde{\boldsymbol{R}}_{i\_Q}$ to the FC.

The channel fading and noises among the SUs and FC directly affect the bit error rate. Then, the messages received by the FC may not be consistent with what SUs sent. However, in most cases, errors do not occur and current encoding schemes generally have error detection and correction capabilities. If errors are detected in the decoding results and can be corrected, the FC can still use the information transmitted by SUs for spectrum sensing without affecting the detection probability of the proposed algorithm. However, it easily incurs additional overhead for error correction. If errors are detected in the decoding results and cannot be corrected, by the delay constraints of spectrum sensing, the FC directly discards the erroneous data and it only processes the transmission data in the remaining SUs. Therefore, it can be assumed that all the data transmitted by the L SUs can reach the FC accurately without any error.

Then Cholesky decomposition is performed for matrices from the SUs to construct residual covariance matrices. Although the absence or presence of PU signals can be determined by (34), (35), and (36), noises have a decisive effect on the detection accuracy at low SNRs. To further improve the detection accuracy at low SNRs, residual covariance matrices by (34) and (35) are proposed. Given that $\tilde{\boldsymbol{R}}_{i\_I}$ and $\tilde{\boldsymbol{R}}_{i\_Q}$ are non-negative symmetric matrices, a unique Cholesky decomposition of the matrix can be expressed as

$$\begin{aligned}\tilde{\boldsymbol{R}}_{i\_I} &= \boldsymbol{B}_{i\_I}\left(\boldsymbol{\Lambda}_{i\_I\_S_{SR}} + \boldsymbol{\Lambda}_{i\_I\_V_{SR}}\right)\boldsymbol{B}_{i\_I}^{H} \\ &= \boldsymbol{U}_{i\_I} \cdot \boldsymbol{U}_{i\_I}^{T} \\ \tilde{\boldsymbol{R}}_{i\_Q} &= \boldsymbol{B}_{i\_Q}\left(\boldsymbol{\Lambda}_{i\_Q\_S_{SR}} + \boldsymbol{\Lambda}_{i\_Q\_V_{SR}}\right)\boldsymbol{B}_{i\_Q}^{H} \\ &= \boldsymbol{U}_{i\_Q} \cdot \boldsymbol{U}_{i\_Q}^{T}, \end{aligned} \tag{38}$$

where there are $\boldsymbol{\Lambda}_{i\_\boldsymbol{S}_{SR}} = diag(\lambda_1, \ldots, \lambda_p, 0, \ldots, 0)_{M\times M}$ and $\boldsymbol{\Lambda}_{i\_\boldsymbol{V}_{SR}} = diag(\gamma \cdot \xi_{i\_n}^2, \gamma \cdot \xi_{i\_n}^2, \ldots, \gamma \cdot \xi_{i\_n}^2)$. γ is the inner product of $cos(wn/f_s)$ or $sin(wn/f_s)$. Then, $\boldsymbol{U}_i$ is represented as

$$\boldsymbol{U}_i = \begin{bmatrix} \sqrt{\lambda_1 + \gamma\xi_{i\_n}^2} & 0 & \cdots & 0 \\ u_{2,1} & \sqrt{\lambda_2 + \gamma\xi_{i\_n}^2} & \cdots & 0 \\ \vdots & \vdots & \ddots & \vdots \\ u_{M,1} & u_{M,2} & \cdots & \sqrt{\gamma\xi_{i\_n}^2} \end{bmatrix}. \tag{39}$$

Authorized licensed use limited to: HANGZHOU DIANZI UNIVERSITY. Downloaded on October 18,2023 at 00:43:50 UTC from IEEE Xplore. Restrictions apply.

The matrices $\boldsymbol{U}_i$ under the above two hypotheses are also different. The matrix $\boldsymbol{U}_i$ obtained by Cholesky decomposition under the hypothesis H_0 and $N \to \infty$ is a diagonal matrix with the same diagonal elements. The diagonal elements are equal to the square root of the noise variance. However, $\boldsymbol{U}_i$ obtained by Cholesky decomposition under the hypothesis H_1 and $N \to \infty$ is a lower triangular matrix with different diagonal elements. The diagonal elements are the square roots of the eigenvalues of the covariance matrix, $i.e.$, the diagonal elements of $\boldsymbol{U}_i$ are $\sqrt{\lambda_s + \lambda_v}$, where λ_s and λ_v are the eigenvalues of the covariance matrices of PU signals and noises, respectively. Since the covariance matrices of PU signals is a non-full-rank matrix, while that of noises is a full-rank one, $i.e.$, the minimum value in the diagonal elements of $\boldsymbol{U}_i$ is $\sqrt{\lambda_v}$. Therefore, the square of the minimum value in the diagonal elements of $\boldsymbol{U}_i$ can be used as an estimate of the noise variance under hypotheses H_0 and H_1. Thus, I/Q residual covariance matrices are calculated as

$$\hat{\boldsymbol{R}}_{i\_I} = \tilde{\boldsymbol{R}}_{i\_I} - \gamma_1 \cdot \xi_{i\_n}^2 \boldsymbol{I}_{M\times M}, \tag{40}$$

$$\hat{\boldsymbol{R}}_{i\_Q} = \tilde{\boldsymbol{R}}_{i\_Q} - \gamma_2 \cdot \xi_{i\_n}^2 \boldsymbol{I}_{M\times M}, \tag{41}$$

where there are $\gamma_1 = \frac{1}{N}\sum_{n=0}^{N-1}\cos^2(\omega n/f_s)$ and $\gamma_2 = \frac{1}{N}\sum_{n=0}^{N-1}\sin^2(\omega n/f_s)$. $\sqrt{\gamma_1 \cdot \xi_{i\_n}^2}$ and $\sqrt{\gamma_2 \cdot \xi_{i\_n}^2}$ are minimum values in diagonal elements of matrices $\boldsymbol{U}_{i\_I}$ and $\boldsymbol{U}_{i\_Q}$ of $\tilde{\boldsymbol{R}}_{i\_I}$ and $\tilde{\boldsymbol{R}}_{i\_Q}$, respectively. The main purpose of residuals on the covariance matrix is to minimize the influence of noises on the characteristics of the covariance matrix of PU signals at low SNRs. Taking a SU with 40 antennas as an example, $\hat{\boldsymbol{R}}_{i\_I}$ and $\hat{\boldsymbol{R}}_{i\_Q}$ of dimension 40×40 under hypotheses H_0 and H_1 are shown in Fig. 6. Physically, residual covariance matrices represent the average power distribution of the PU signals received by the SU antennas. For example, the elements in coordinate of (i, j) in subplots 6(a) and subplots 6(c) represent the average power of I phase signals received by i-th and j-th antennas. Given the hypothesis H_0, as there are no PU signals, the value for each element in residual covariance matrices is 0. The value of each element in residual covariance matrices is the mean power of PU signals in received signals under the hypothesis H_1. The darker color of grids in Fig. 6, the smaller values they represent. The darker diagonals of the four matrices are caused by matrix cancellation. $\hat{\boldsymbol{R}}_{i\_I}$ and $\hat{\boldsymbol{R}}_{i\_Q}$ under hypotheses H_0 and H_1 can be easily distinguished.

Then, $\gamma_1 \cdot \xi_{i\_n}^2$ and $\gamma_2 \cdot \xi_{i\_n}^2$ are also used for the credibility of the i-th SU, which is expressed as

$$\varphi_{i\_I} = \frac{s_{i\_I\_power}}{\gamma_1 \cdot \xi_{i\_n}^2}$$

$$s_{i\_I\_power} = \frac{1}{M(M-1)}\sum_{m}^{M}\sum_{n}^{M}\hat{\boldsymbol{R}}_{i\_I}(m,n), (m \neq n), \tag{42}$$

$$\varphi_{i\_Q} = \frac{s_{i\_Q\_power}}{\gamma_2 \cdot \xi_{i\_n}^2}$$

$$s_{i\_Q\_power} = \frac{1}{M(M-1)}\sum_{m}^{M}\sum_{n}^{M}\hat{\boldsymbol{R}}_{i\_Q}(m,n), (m \neq n). \tag{43}$$

The physical nature of the covariance matrix is the energy distribution relationship of received signals. The credibility φ_i derived from s_{i_power} and $\gamma \cdot \xi_{i\_n}^2$ has similar transformation trend as the SNR, thus it indirectly reflects the SNR in the environment, where the i-th SU is located. The credibility weights are then calculated as

$$w_{i\_I} = \frac{\varphi_{i\_I}}{\sum_{k=1}^{L}\varphi_{k\_I}}, \tag{44}$$

$$w_{i\_Q} = \frac{\varphi_{i\_Q}}{\sum_{k=1}^{L}\varphi_{k\_Q}}. \tag{45}$$

According to (44) and (45), the SUs with better communication environment are given larger weights.

Finally, the residual covariance matrices of the SUs are fused with different weights in the fusion center as

$$\begin{aligned}\boldsymbol{R}_{fusion\_I} &= \sum_{i=1}^{L} w_{i\_I}\hat{\boldsymbol{R}}_{i\_I} \\ &= \frac{1}{N}\sum_{i=1}^{L}\sum_{k=1}^{N} w_{i\_I}\, y_{i\_SR\_I}(k) y_{i\_SR\_I}^H(k),\end{aligned} \tag{46}$$

$$\begin{aligned}\boldsymbol{R}_{fusion\_Q} &= \sum_{i=1}^{L} w_{i\_Q}\hat{\boldsymbol{R}}_{i\_Q} \\ &= \frac{1}{N}\sum_{i=1}^{L}\sum_{k=1}^{N} w_{i\_Q}\, y_{i\_SR\_Q}(k) y_{i\_SR\_Q}^H(k),\end{aligned} \tag{47}$$

where $\boldsymbol{R}_{fusion\_I}$ and $\boldsymbol{R}_{fusion\_Q}$ are fusion matrices of $\hat{\boldsymbol{R}}_{i\_I}$ and $\hat{\boldsymbol{R}}_{i\_Q}$. The credibility weighted matrix fusion can not only improve the average SNR of the SUs, but also reduce the errors caused by progressive statistic theory. For example, suppose that there are three SUs in CRNs and the credibility in covariance matrices of the SUs is 1, 1 and 0.5, respectively. Here, the credibility is the ratios of the PU energy to noises. In the fusion matrix, the credibility is obtained as 9/12 by directly averaging the covariance matrices of the SUs, while that is obtained as 10/12 by credibility weighting. Larger credibility in the fusion matrix leads to easier detection of PU signals in received signals under the hypothesis H_1. If the credibility of the above three SUs is 1, 1 and 1, respectively, the credibility weighted matrix fusion is equivalent to directly averaging covariance matrices. It is also better than independent decision-making by a single SU. Eqs. (46) and (47) are simplified to $(\sum_{i=1}^{L}\sum_{k=1}^{N} y_{i\_SR}(k) y_{i\_SR}^H(k))/LN$. The credibility weighted matrix fusion is equivalent to the changes of the length of received signals from N to LN. But it does not increase the sensing slot. When $L \to \infty$, it is regarded as $\boldsymbol{R}_{i\_I} = \tilde{\boldsymbol{R}}_{i\_I}$ and $\boldsymbol{R}_{i\_Q} = \tilde{\boldsymbol{R}}_{i\_Q}$ in (37).

B. Stochastic Resonance and Parameter Optimization

In [21], the SNR of the SR output, $i.e.$, SNR_{out}, is an identification to judge whether the resonance phenomenon occurs and optimizes parameters a and b in terms of stochastic resonance theory. According to the adiabatic approximation theory [32], the SNR of output signals of a bistable SR system is calculated as

Authorized licensed use limited to: HANGZHOU DIANZI UNIVERSITY. Downloaded on October 18,2023 at 00:43:50 UTC from IEEE Xplore. Restrictions apply.

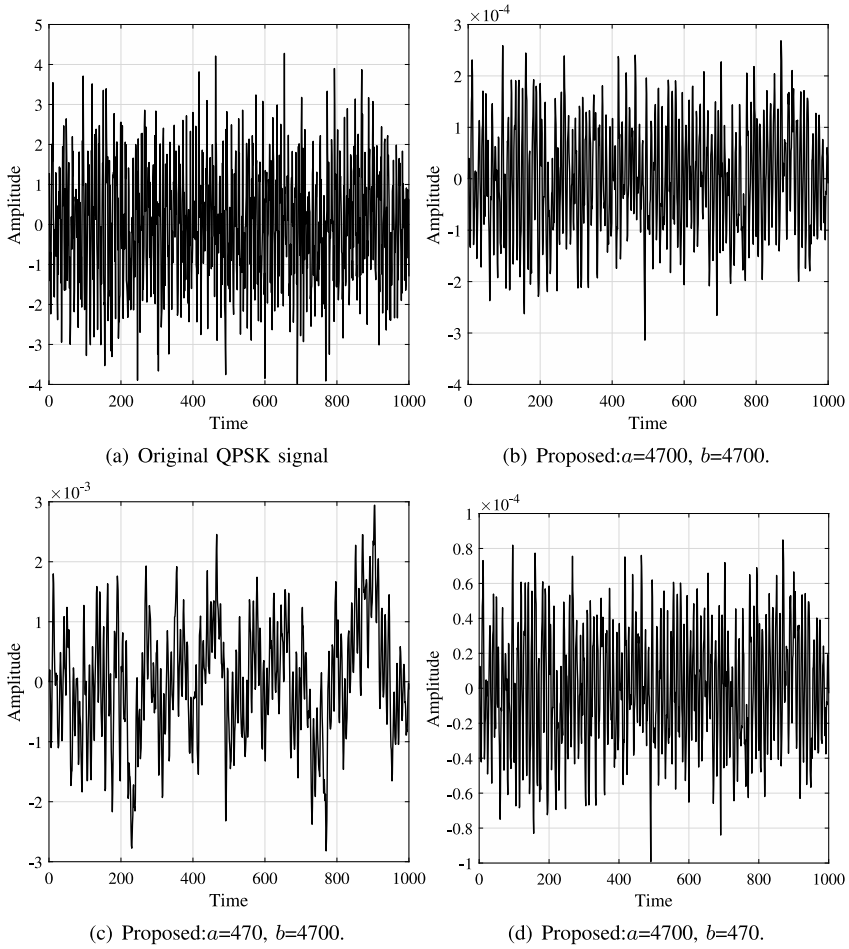

(a) Original QPSK signal (b) Proposed:a=4700, b=4700.

(c) Proposed:a=470, b=4700. (d) Proposed:a=4700, b=470.

Fig. 7. Different effects of parameter a and b on the SR system output.

$$SNR_{out} = \sqrt{2}\Delta U\left(\frac{A}{D}\right)^2 \exp\left(-\frac{\Delta U}{D}\right), \tag{48}$$

where A is the amplitude of the PU signals. When the noise intensity D increases, SNR_{out} does not decrease monotonically, but it first increases and then decreases. Given $D = \Delta U/2$, SNR_{out} reaches its maximum value as $SNR_{out} = 4\sqrt{2}A^2\exp(-2)/\Delta U$. In the PNBSR, there is $\Delta U = a^4/12b^3$, while there is $\Delta U = a^2/4b$ in the TBSR. Given $a = b$, the SNR of output signals of the PNBSR is larger than that of the TBSR. Therefore, the parameters a and b in the stochastic resonance can be indirectly solved with (8) and (14) by the maximization of SNR, *i.e.*,, the following optimization objective function, as

$$\max SNR_{out} = \frac{\lim_{N\to\infty}\frac{1}{N}\sum_{n=0}^{N-1}\|s_{SR}(n)\|^2}{\lim_{N\to\infty}\frac{1}{N}\sum_{n=0}^{N-1}\|v_{SR}(n)\|^2} = \frac{\sigma^2_{s(SR)}}{\sigma^2_{v(SR)}}. \tag{49}$$

When SNR_{out} reaches its maximum, PU signals and noises are considered to produce the SR [27]. However, the calculation of SNR_{out} requires prior information or complex estimation algorithms [33]. Therefore, by the characteristics of the covariance matrix $\tilde{\boldsymbol{R}}_{\boldsymbol{Y_{SR}}}$, a new optimization objective function ψ is employed to replace SNR_{out} in (49) to obtain the optimal a and b with (8) and (14). And it is presented as

$$\max\psi = \frac{\frac{1}{M^2-M}\sum_{l=1}^{M}\sum_{l\neq p}\tilde{\boldsymbol{R}}_{\boldsymbol{Y}_{SR}}(l,p)}{\frac{1}{M}\sum_{l=1}^{M}\tilde{\boldsymbol{R}}_{\boldsymbol{Y}_{SR}}(l,l)}, \tag{50}$$

where $\tilde{\boldsymbol{R}}_{\boldsymbol{Y}_{SR}}(l,p)$ is an element with coordinate (l, p) of $\tilde{\boldsymbol{R}}_{\boldsymbol{Y}_{SR}}$. According to (26), $\boldsymbol{R}_{\boldsymbol{Y}_{SR}}$ is divided into $\boldsymbol{R}_{\boldsymbol{S}_{SR}}$ and $\boldsymbol{R}_{\boldsymbol{V}_{SR}}$. Each element in $\boldsymbol{R}_{\boldsymbol{S}_{SR}}$ is the inner product of the same PU signal. $\boldsymbol{R}_{\boldsymbol{V}_{SR}}$ is $\xi_n^2\boldsymbol{I}_{M\times M}$. Thus, $\frac{1}{M^2-M}\sum_{l=1}^{M}\sum_{l\neq p}\tilde{\boldsymbol{R}}_{\boldsymbol{Y}_{SR}}(l,p)$ is approximately equal to $\frac{1}{N} < s_{SR}(n)\cdot s_{SR}(n) >$ and $\frac{1}{M}\sum_{l=1}^{M}\tilde{\boldsymbol{R}}_{\boldsymbol{Y}_{SR}}(l,l)$ is approximately equal to $\frac{1}{N} < s_{SR}(n)\cdot s_{SR}(n) > +\xi_n^2$. When parameters a and b are adjusted to maximize SNR_{out}, ψ reaches a maximum at the same time. Eq. (50) is easier to be calculated, when compared with (49) and requires no prior information. Then the artificial fish swarm algorithm [34], with specified parameters shown in Table I, is used to find the optimal parameters a and b in (50) as an objective function.

In Fig. 7, subplot 7(a) is a received signal and subplot 7(b) is an output of the PNBSR under the optimal a and b. After changing a, the output is shown in subplot 7(c) and the PU signal is distorted. However, if only b is changed in subplot 7(d), the output remains the same except in amplitude compared with subplot (b). The experimental result shows that the SR phenomenon mainly depends on the parameter

Authorized licensed use limited to: HANGZHOU DIANZI UNIVERSITY. Downloaded on October 18,2023 at 00:43:50 UTC from IEEE Xplore. Restrictions apply.

TABLE I
ARTIFICIAL FISH SWARM PARAMETERS

Fish Number	100
Iterations	20
Try Number	20
Delta	0.618
Visual	f_s^{-1}
Step	$0.5 \times f_s \times 10^{-1}$

a, while the parameter b only changes the amplitude of the output. Owing to normalization, the influence of amplitude on algorithm performance can be ignored. Thus, the TBSR and PNBSR in SR systems are applicable to PU signals with no frequency changes within one detection cycle. Therefore, to simplify the optimization, we make b equal to a.

C. Classification of PUs and Noises by the CNN

The CNN obtains strong learning ability about matrix type feature statistics, and it is used to solve the optimal decision boundary of residual covariance matrices under hypotheses H_0 and H_1. The structure of the CNN determines the ability of the CNN to extract features and it needs to match the data sets. For simple data, overfitting occurs if the CNN with a complex structure is adopted. Otherwise, underfitting occurs.

First, several samples $(\boldsymbol{x}_1, y_1), \ldots, (\boldsymbol{x}_G, y_G), \mathbf{x}_i \in \boldsymbol{R}_{2\times M\times M}$ are set as training data, and $y_i \in \{+1, -1\}$ is the label of $\boldsymbol{x}_i$. The dimension of the CNN input is $2 \times M \times M$, and G is the sample number. Thus, the output of the L-th convolution layer of the CNN is expressed as

$$\boldsymbol{X}^{(L)} = f\left(\boldsymbol{w}^{(L)} \otimes \boldsymbol{X}^{(L-1)} + \boldsymbol{b}^{(L)}\right), \tag{51}$$

$$f(x) = relu(x) = \begin{cases} x & x \geq 0 \\ 0 & x < 0 \end{cases}, \tag{52}$$

where $\boldsymbol{w}^{(L)}$ is the convolution kernel of the L-th convolution layer. To learn training samples, the loss function in the proposed scheme is represented as

$$g_{w,b}(\boldsymbol{x}_i) = \hat{y}_i, \tag{53}$$

$$Loss = -\sum_{i=1}^{G} y_i \log(\hat{y}_i) + (1 - y_i)\log(1 - \hat{y}_i), \tag{54}$$

where $g_{W,b}(\cdot)$ is the mapping relationship between training samples and labels. $\hat{y}_i$ is the label predicted by the CNN.

Then, according to actual simulation results, the specific framework of the CNN used in this study is given in Table II. The CNN includes four convolution layers, three maxpool layers and one denser layer. The probabilities of "+1" and "−1" are given by the denser layer. Finally, whether there is a PU signal is determined according to the set threshold and the probabilities of "+1" and "−1".

D. Flow Chart of the Proposed Spectrum Sensing

The proposed scheme pre-processes received signals with the PNBSR to improve the SNRs. The Cholesky decomposition-based matrix cancellation is used to construct I/Q residual covariance matrices. Then, the credibility weighted matrix fusion is performed to fuse residual covariance matrices of the SUs for cooperation. Finally, a CNN is trained and tested, and then the trained CNN is used for spectrum sensing. In summary, the entire process of the proposed scheme is shown in Fig. 8 and illustrated as follows.

TABLE II
CNN PARAMETERS

Layer	Shape	Stride	Activation
l_1: Convolution Layer	$30 \times 2 \times 2 \times 2$	1	Relu
l_2: Maxpool Layer	2×2	1	/
l_3: Convolution Layer	$60 \times 2 \times 2$	1	Relu
l_4: Maxpool Layer	2×2	1	/
l_5: Convolution Layer	$100 \times 2 \times 2$	1	Relu
l_6: Maxpool Layer	2×2	1	/
l_7: Convolution Layer	$128 \times 2 \times 2$	1	Relu
l_8: Denser Layer	2	1	Sigmoid

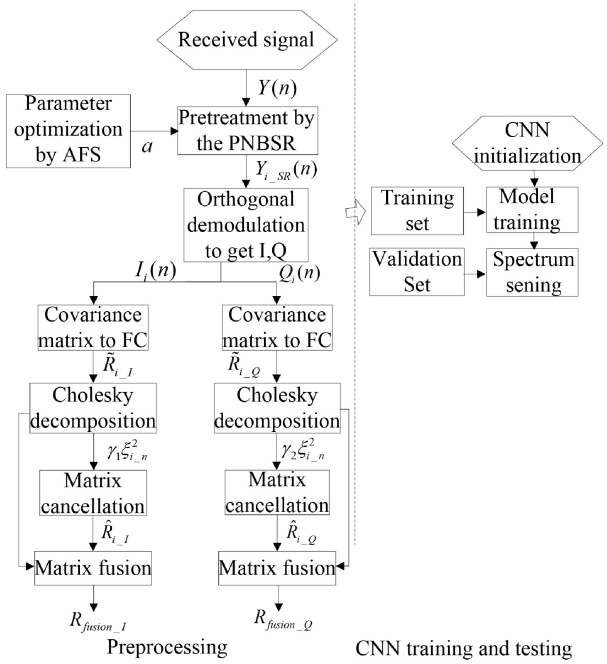

Fig. 8. Flow chart of the proposed cooperative spectrum sensing with the PNBSR-CNN-based residual covariance matrices.

Step 1). The PNBSR system with optimal parameters is used to preprocess received signal matrices, which transfers parts of energy in noises to PU signals for higher quality signals and greatly reduces the interference of noises in the detection to improve the detection accuracy at low SNRs. Then, orthogonal demodulation is performed on the output signals to obtain the strengthened I/Q matrices.

Step 2). Next, I and Q phase covariance matrices are constructed in the SU and sent to the FC. To further improve the detection accuracy at low SNRs, matrix cancellation by using Cholesky decomposition is proposed to construct residual covariance matrices $\hat{\boldsymbol{R}}_{i\_I}$ and $\hat{\boldsymbol{R}}_{i\_Q}$. At low SNRs, the noise variance predominates in covariance matrices. Thus,

Authorized licensed use limited to: HANGZHOU DIANZI UNIVERSITY. Downloaded on October 18,2023 at 00:43:50 UTC from IEEE Xplore. Restrictions apply.

matrix cancellation can reduce the influence of noises on covariance matrices to improve detection accuracy.

Step 3). Then, the credibility weighted matrix fusion is carried out for $\boldsymbol{R}_{fusion\_I}$ and $\boldsymbol{R}_{fusion\_Q}$ to improve the average SNR of the SUs and it reduces the calculation error of sample covariance matrices.

Step 4). According to steps 1) to 3), training and test samples composed of residual covariance matrices and the corresponding labels are generated. Then, the CNN is trained by the training samples to generate the spectrum classifier.

Step 5). The residual covariance matrices of test samples are input into the spectrum sensing classifier generated in Step 4). If the output is"+1," the PU signal is present. Otherwise, it is absent.

In short, the proposed cooperative spectrum sensing is implemented as follows. First, a PNBSR system is adopted to improve the SNR of received signals. Second, I/Q covariance matrices of strengthened signals are calculated in each SU. The noise variance of each SU is estimated by the Cholesky decomposition to construct I/Q residual covariance matrices for better performance. Third, residual covariance matrices from the different SUs are integrated with credibility weighted matrix fusion in the FC. Hypotheses H_1 and H_0 are labeled with "+1" and "−1," respectively. Then a CNN classifier is generated by training labels and corresponding statistics. Finally, the test samples are input into the classifier. If the output is "+1," the spectrum of the PU is occupied. Otherwise, it is not occupied and free for use.

E. Computational Complexity Analyses

The computational complexity of the proposed spectrum sensing scheme is analyzed in two aspects.

First, the complexity of the proposed scheme used for single-user independent detection mainly lies in following three aspects. The first is to process the received signal matrices with the PNBSR, where $17(N-1)M$ multiplications and $15(N-1)M$ additions are required. Here, M and N are the number of antennas in a SU and that of sampling points in one observation is obtained in a sensing slot. During the setting of system parameters, the complexity of the proposed model ψ in Section III is estimated as $o(M^2)$. Compared with the traditional model's SNR_{out}, the complexity of which is $o(M^3)$, the proposed model considerably improves the speed of optimizing parameter a. The second aspect is the computation of the residual covariance matrices. Although the MME, GEMD [35], SVM [18], CNN [19] and the proposed scheme are all required to compute the covariance matrix, the complexity of which is $M(M+1)N/2$ multiplications and $M(M+1)(N-1)/2$ additions. The proposed scheme divides signals into orthogonal I/Q signals, so that the computational complexity of the covariance matrix is twice as much as others and $M(M+1)N$ multiplications and $M(M+1)(N-1)$ additions are required. Compared with the MME, GEMD and SVM schemes, the proposed scheme performs the Cholesky decomposition with double complexity $o(2M^3/3)$ to construct the residual covariance matrices. The third aspect is the use of the trained CNN model to be classified. And this process needs $o(\sum_{k=1} P_k^2 G_k^2 U_k U_{k-1})$ multiplications and $o(\sum_{k=1} P_k^2 (G_k^2-1) U_k U_{k-1})$ additions. Here, P_k, G_k and U_k represent the length of the output feature graph, the convolution kernel length and the number of output channels of the k-th convolution layer, respectively. Compared with the SVM, the complexity of which is $o(NN_s)$, the CNN model is more suitable for high dimensional data and it has stronger classification ability. Here, N_s represents the number of support vectors. In conclusion, the computational complexity of the proposed scheme is compared with other methods in Tabs. III and IV.

TABLE III
COMPARISON OF COMPUTATIONAL COMPLEXITY IN MULTIPLICATIONS AMONG THE PROPOSED AND EXISTING SPECTRUM SENSING METHODS

Algorithm	Complexity in Multiplications
ED	MN
MME	$N(M+1)M/2+o(M^3)$
GEMD	$N(M+1)M/2+o(M^3)$
SVM	$N(M+1)M/2+o(M^3+NN_s)$
CNN	$N(M+1)M+o(\sum_{k=1} P_k^2 G_k^2 U_k U_{k-1})+o(2M^3/3)$
Proposed	$N(M+16)M+o(\sum_{k=1} P_k^2 G_k^2 U_k U_{k-1})+o(2M^3/3)$

TABLE IV
COMPARISON OF COMPUTATIONAL COMPLEXITY IN ADDITIONS AMONG THE PROPOSED AND EXISTING SPECTRUM SENSING METHODS

Algorithm	Complexity in Additions
ED	$M(N-1)$
MME	$(N-1)(M+1)M/2+o(M^3/3)$
GEMD	$(N-1)(M+1)M/2+o(M^3/3)$
SVM	$(N-1)(M+1)M/2+o(M^3/3+NN_s)$
CNN	$(N-1)(M+1)M+o(\sum_{k=1} P_k^2 (G_k^2-1) U_k U_{k-1})$
Proposed	$(N+11)(M+1)M+o(\sum_{k=1} P_k^2 (G_k^2-1) U_k U_{k-1})$

Second, the above content is the complexity analysis of the proposed scheme in the case of the single-user detection. Next, the complexity of the proposed cooperative spectrum sensing scheme compared with traditional cooperation is analyzed. The traditional cooperation, decision fusion, including logical-OR rule, logical-AND rule, and K-rule are widely used. However, the complexity of the traditional one is proportional to the number of the SUs by this method. Suppose that L SUs are presented in a CRN, if the proposed cooperative spectrum sensing scheme relies on decision fusion, its complexity is $L(N(M+16)M+o(\sum_{k=1} P_k^2 G_k^2 U_k U_{k-1})+o(2M^3/3))$ multiplications and $L((N+11)(M+1)M+o(\sum_{k=1} P_k^2 (G_k^2-1) U_k U_{k-1}))$ additions. However, the matrix fusion reduces the complexity by removing considerable repetition and the complexity of the total scheme is $LN(M+16)M+o(\sum_{k=1} P_k^2 G_k^2 U_k U_{k-1})+o(2LM^3/3)$ multiplications and $L((N+11)(M+1)M+(L-1)M^2)+o(\sum_{k=1} P_k^2 (G_k^2-1) U_k U_{k-1})$ additions.

In summary, the proposed algorithm increases in complexity when compared with the existing spectrum sensing

Authorized licensed use limited to: HANGZHOU DIANZI UNIVERSITY. Downloaded on October 18,2023 at 00:43:50 UTC from IEEE Xplore. Restrictions apply.

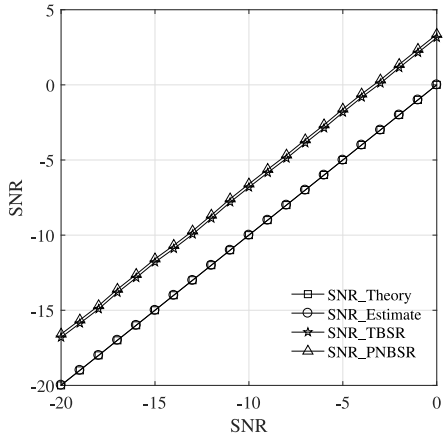

Fig. 9. The SNR enhancement performance of the SR.

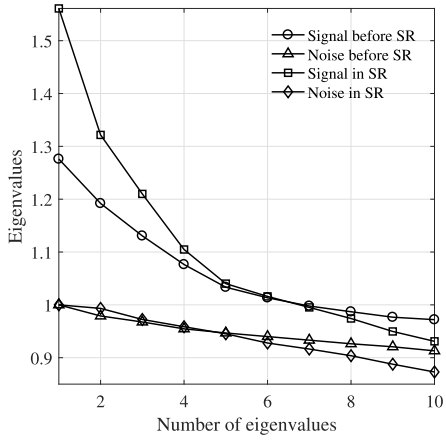

Fig. 10. The changing process of the eigenvalues of signals in the PNBSR system.

methods. However, the detection probability of the proposed algorithm is obviously improved at the cost of these acceptable complexity growth.

IV. Simulation and Result Analysis

The performance of the proposed cooperative spectrum sensing scheme is mainly verified by numerical simulations, and experimental parameters are listed as follows. QPSK modulation is adopted to modulate PU signals. The AWGN is applied with zero mean and variance σ_n^2. Suppose that different SNR conditions in a real communication environment are simulated by changing σ_n^2. The number of antennas of the SUs is set as 10. The frequency of PU signals is set as $f_c = 1 \times 10^3$ Hz, and the sampling frequency is $f_s = 1 \times 10^4$ Hz. The sampling interval is $T = 0.1s$. A total of 2000 training samples and 1000 test samples are generated at each SNR to train and test the CNN model. In each of the following experiments, if experimental parameters change, they are explained separately.

A. Analysis of the SR System and Noise Estimation

In Section III, the PNBSR has a lower potential well barrier and flatter potential well wall to bring a better enhancement than that of the TBSR in (48). Then, the performance of the two SR models is compared together in Fig. 9. The TBSR improves the SNR of the received signals by about 3.14dB. The enhancement of the PNBSR outperforms that of the TBSR by 0.22dB.

According to the above results, the eigenvalues of covariance matrices of received signals are compared before and after the PNBSR treatment in Fig. 10.

In Fig. 10, when received signals are noises, the SR cannot be generated, and no obvious difference is found between the eigenvalues of output signals and received signals. When received signals include both PU signals and noises, the first five eigenvalues of the received signal matrix contain the energy of both PU signals and noises, while the last five ones only contain the energy of noises. Then, PU signals and noises produce the SR in the PNBSR with the optimal a. Comparing the eigenvalues of the input and output shows that the PNBSR reduces the eigenvalues of noise and increases those of PU signals. Therefore, the PNBSR with the optimal a transfers part of the energy of noises to PU signals.

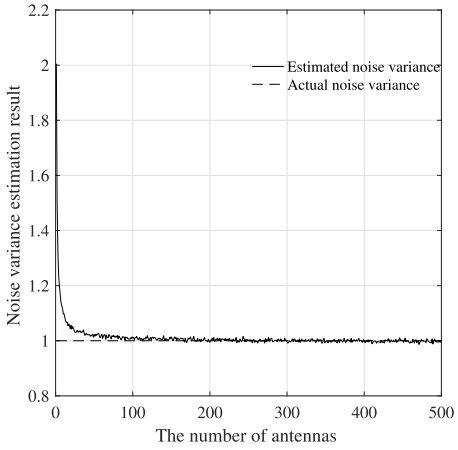

Fig. 11. The impact of the number of antennas on the estimated noise variance.

Since the noise variance estimation is required to reduce the impact of noises on the detection statistics, the estimation of the noise variance can improve the detection accuracy of the proposed spectrum sensing scheme. Then, assuming the amplitude of the PU signal as 1 and the noise variance as 1, the impact of the number of antennas on the estimated noise variance is simulated numerically in Fig. 11. With more antennas, the estimated noise variance is much closer to the actual one.

Because the robustness of the proposed cooperative spectrum sensing mainly depends on the PNBSR, the influence of the system parameter a on the enhancement effect is simulated and plotted in Fig. 12.

In Fig. 12, the influence of the parameter a on the enhancement under three SNRs and two PU frequencies is exhibited. The parameter a is normalized. In Fig. 12, although there is only one optimal parameter a for each PU signal frequency, the SNR gain is still larger than 0 during 85% adjustment intervals near a. Hence, the PNBSR has strong robustness.

Authorized licensed use limited to: HANGZHOU DIANZI UNIVERSITY. Downloaded on October 18,2023 at 00:43:50 UTC from IEEE Xplore. Restrictions apply.

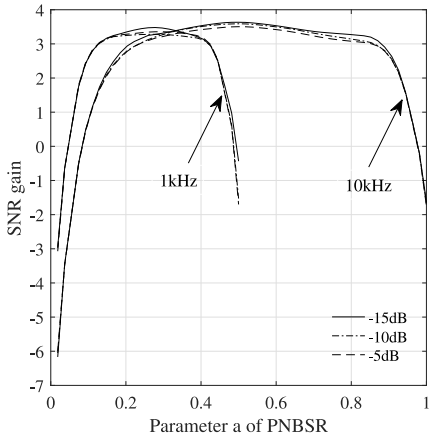

Fig. 12. The corresponding relationship between the enhancement and the parameter a.

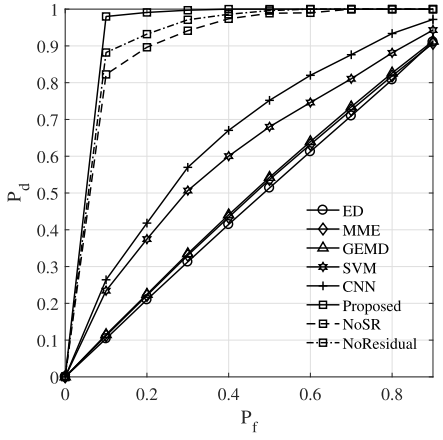

Fig. 14. Comparison of ROC curves of different spectrum sensing schemes at -13 dB.

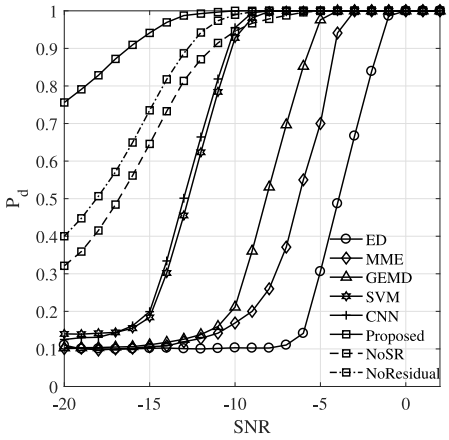

Fig. 13. Comparison of detection probabilities of different spectrum sensing schemes.

B. Performance Comparison Among the Proposed Spectrum Sensing Scheme and Other Schemes

Next, in the case of different SNRs and false alarm probabilities P_f, the detection probabilities P_d of the ED, MME, GEMD, SVM, CNN and proposed schemes with one SU are simulated and compared. The performance of the proposed scheme without the PNBSR and matrix cancellation is compared.

In Fig. 13, the detection probability of each spectrum-sensing scheme at different SNRs under false alarm probability of 0.1. The detection probabilities of the proposed, CNN, and SVM schemes are also better than those of conventional spectrum detection schemes, because the decision thresholds of the traditional ED and schemes based on eigenvalues are so progressive that the decision thresholds with large errors cannot accurately detect PU signals from noises at low SNRs. However, three intelligent algorithms automatically give more accurate decision thresholds from the CNN or SVM model with the actual data. Compared with the SVM scheme, the detection probabilities of the CNN and proposed schemes are improved by 1 dB and 2dB, respectively, when the detection probability of the SVM scheme is 1 at SNR of -8 dB. At -15 dB, the detection accuracy of the proposed algorithms is 77% and 75% higher than those of the SVM and CNN schemes, respectively. This phenomenon can be explained as follows. First, the SVM detection method is based on eigenvalues. Although it solves the problem of the imprecise threshold, the SVM scheme only uses the eigenvalues of the covariance matrix and it does not make full use of all the information carried by the covariance matrix. Also the CNN has more advantages than the SVM in dealing with high-dimensional data. Second, compared with the CNN scheme, the proposed scheme introduces a PNBSR system in (21) to improve the SNR of received signals. In addition, the matrix cancellation operation of (40) and (41) is proposed to construct residual covariance matrices, thereby weakening the interference of noises in the detection and making PU signals dominant in covariance matrices. Then residual covariance matrices are used to train the CNN to make the weights in (51) more sensitive to PU signals, thereby improving the detection accuracy at low SNRs. Therefore, the proposed scheme is superior to traditional schemes and other intelligent schemes in terms of detection probability. Since Fig. 9 shows that the PNBSR improves the SNR of the received signals by about 3.36dB, it is also verified in Fig. 13 that the PNBSR significantly improves the detection performance of the proposed algorithm. Due to the sensitivity of the CNN to numerical values, the matrix cancellation to eliminate the noise interference is necessary to improve the detection performance too.

The receiver operating characteristic (ROC) curve is another effective tool to evaluate the spectrum sensing performance. Fig. 14 shows the ROC curves of various schemes at an SNR of -13 dB.

In Fig. 14, a positive correlation trend occurs between detection probability and false alarm probability. Three intelligent methods perform better than those of the ED, MME and GEMD in terms of the ROC at -13 dB. In particular, the detection probability of the proposed algorithm reaches 0.98, when the false alarm probability is 0.1. Compared with the other two intelligent algorithms, the proposed scheme reduces the false alarm probability by at least 60%, when the detection probability is 0.9. In summary, three intelligent algorithms achieve higher performance in comparison with the traditional algorithms owing to the more accurate decision threshold

Authorized licensed use limited to: HANGZHOU DIANZI UNIVERSITY. Downloaded on October 18,2023 at 00:43:50 UTC from IEEE Xplore. Restrictions apply.

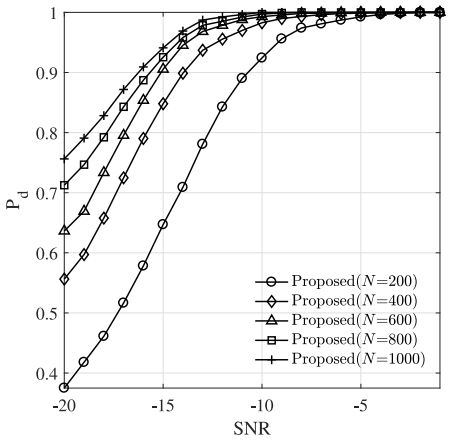

Fig. 15. Influence of the number of sampling points on the detection probability of the proposed algorithm.

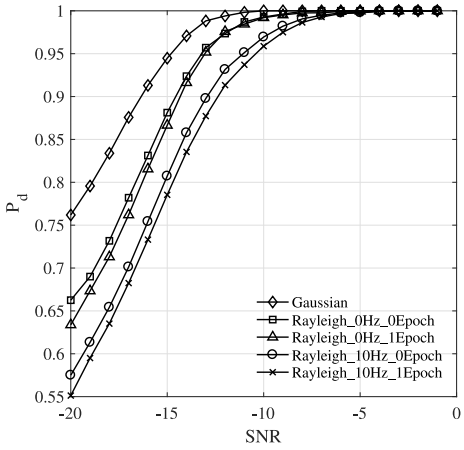

Fig. 16. Influence of the different channel conditions on the detection probability of the proposed algorithm.

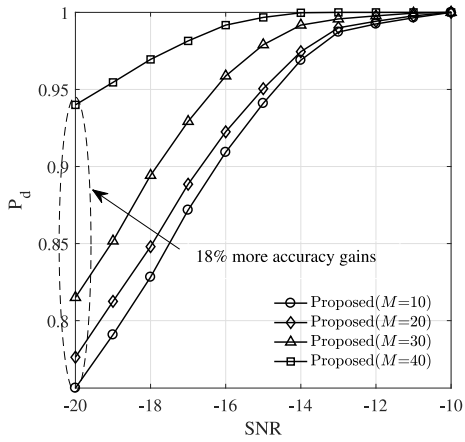

Fig. 17. Influence of the number of antennas on the detection probability for the proposed scheme.

generated by the SVM and CNN models, whereas the CNN classifier achieves a higher detection probability by making full use of the covariance matrix. A PNBSR system and matrix cancellation are adopted in the proposed scheme to further improve the detection probability in (21), (40) and (41). Thus, the proposed scheme obtains a better detection performance compared with those of the other two intelligent schemes.

In Fig. 15, the detection probability of the proposed scheme by a single SU increases with the increase of sampling points N in the range from 200 to 1000. The performance improvement caused by increasing the same number of sampling points decreases gradually. The reason for this phenomenon is explained as follows. When the number of sampling points increases gradually and $N \to \infty$, the sample covariance matrices gradually approximates the statistical covariance matrices in terms of (37), thereby reducing the calculation error and making the actual performance of the proposed algorithm closer to the best theoretical performance. However, while improving the detection performance, the increase in sampling points leads to more complex calculations and higher latency.

Fig. 16 simulates the impact of different channel conditions on the detection probability of the proposed algorithm. The channels are selected as the Gaussian and Rayleigh channels. The maximum frequency offset in the Rayleigh channel is 10 Hz and the maximum delay is one period for the PU signals.

In Fig. 16, the detection probability of the proposed algorithm in Gaussian channels is higher than that in Rayleigh channels. This is due to the presence of fading coefficients in Rayleigh channels, which reduces the autocorrelation and cross-correlation of PU signals, causing the detection statistics in (40) and (41) under the hypothesis H_1 more similar to those of random variables. Moreover, the Doppler frequency shift and delay in the Rayleigh channels reduce the detection probability in the proposed algorithm. Because the Doppler frequency shift and delay reduce the cross-correlation among signals received by different antennas. When a Doppler frequency shift occurs, according to trigonometric functions, the covariance among signals received by different antennas approaches zero. When the delay of the PU signals received by two antennas is exactly $\pi/2$, the PU signals are orthogonal and the above covariance is zero too.

The number of antennas in contemporary wireless devices is increasing gradually. Then, the influence of the number of antennas from 10 to 40 on the detection probability is simulated in Fig. 17. As the number of antennas in a SU increases, the detection probability is increasing. Furthermore, the detection probability increases by 18% by the scheme of 40 antennas, compared with that of the same scheme of 10 ones at -20 dB. The number of antennas determines the dimension of the detection statistics, and a larger dimension exhibits that the CNN learns much more from the detection statistics to obtain a more accurate classifier. Moreover, as the number of antennas increases, the accuracy of noise variance estimation improves too. By the construction of the residual covariance matrices, the interference caused by the noises in the detection statistics can be removed to the greatest extent, thereby improving the detection probability of the proposed algorithm. However, at the same time, it requires that the CNN has a strong learning ability to be equipped with more complex model structures. Hence, the performance improvement brought by the larger dimension statistics is obtained at the cost of a large amount of computation.

Then, the proposed scheme and the K-rule one are compared when the number of the SUs cooperating with each

Authorized licensed use limited to: HANGZHOU DIANZI UNIVERSITY. Downloaded on October 18,2023 at 00:43:50 UTC from IEEE Xplore. Restrictions apply.

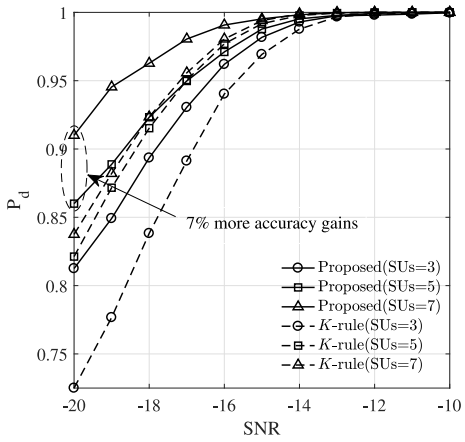

Fig. 18. Comparison of detection probabilities of different cooperative spectrum detection schemes.

other is 3, 5, and 7. In Fig. 18, with the same number of the SUs, the credibility weighted matrix fusion has better detection performance compared with the K-rule at low SNRs. In particular, the credibility weighted matrix fusion improves the detection probability by 7% at -20 dB under 7 SUs. Although the detection performance of two cooperative schemes improves with the increase of the number of the SUs, the performance improvement of the K-rule is not obvious, when the number of the SUs increases from 5 to 7. The reason for this result is listed as follows. The K-rule scheme adopts the voting idea of the minority obeying the majority to reduce the probability of the detection error caused by the sudden deterioration. Then, the detection performance is indirectly improved by reducing the probability of the detection error. However, when the number of the SUs is 5, the detection error is reduced to be sufficiently small. It is actually the algorithm itself that ultimately limits the performance. For the proposed matrix fusion in (46) and (47), it applies different weights to different SUs according to the credibility of them to improve the average SNR. When the credibility of the SUs is the same, the credibility weighted matrix fusion is equivalent to the increase of the number of sampling points. So, the sample covariance matrix is closer to the statistical covariance matrix. When the channel fading and noise among SUs and FC cause a decrease in the number of the SUs participating in cooperation, it ultimately reduces the detection accuracy of the proposed cooperative spectrum sensing scheme.

V. Conclusion

A novel piecewise normalized bistable stochastic resonance strengthened cooperative spectrum sensing with the CNN and residual covariance matrices is proposed to improve the detection accuracy for SUs at low SNRs in wireless communications. The advantages are presented as follows. First, a PNBSR system is proposed to improve the SNR of received signals and it performs better than those of the TBSR system. In the PNBSR, a new optimization index is proposed to optimize system parameters more easily. Second, Cholesky decomposition-based matrix cancellation and the credibility weighted matrix fusion are proposed to reduce calculation errors and noise interference for higher detection accuracy. Third, a CNN model is used to immediately determine the existence of the PUs. The decision threshold of the proposed algorithm is completely learned by the CNN. Finally, at low SNRs, the spectrum sensing performance of the proposed scheme is better than those of other detection schemes in terms of detection probabilities. Simulation results indicate that the proposed scheme achieves significant improvement in terms of the detection accuracy at low SNRs and it has strong robustness to cope with the channel fading, which verify its suitability in 5G communications.

References

[1] N. Tadayon and S. Aissa, "A multichannel spectrum sensing fusion mechanism for cognitive radio networks: Design and application to IEEE 802.22 WRANs," *IEEE Trans. Cogn. Commun. Netw.*, vol. 1, no. 4, pp. 359–371, Dec. 2015.

[2] A. Zaeemzadeh, M. Joneidi, N. Rahnavard, and G.-J. Qi, "Co-SpOT: Cooperative spectrum opportunity detection using Bayesian clustering in spectrum-heterogeneous cognitive radio networks," *IEEE Trans. Cogn. Commun. Netw.*, vol. 4, no. 2, pp. 206–219, Jun. 2018.

[3] M. McHenry and S. Karl, *NSF Spectrum Occupancy Measurements*, Shared Spectr. Company, Vienna, VA, USA, Oct. 2005.

[4] J. Mitola and G. Q. Maguire, "Cognitive radio: Making software radios more personal," *IEEE Pers. Commun.*, vol. 6, no. 4, pp. 13–18, Aug. 1999.

[5] F. F. Digham, M. S. Alouini, and M. K. Simon, "On the energy detection of unknown signals over fading channels," in *Proc. IEEE Int. Conf. Commun. (ICC)*, vol. 5. Anchorage, AK, USA, Jan. 2003, pp. 21–24.

[6] Y. Long, Q. Wu, and J. Wang, "Optimal adaptive multi-band spectrum sensing in cognitive radio networks," *KSII Trans. Internet Inf. Syst.*, vol. 8, no. 3, pp. 984–996, Mar. 2014.

[7] W. Gardner, "Spectral correlation of modulated signals: Part I—Analog modulation," *IEEE Trans. Commun.*, vol. 35, no. 6, pp. 584–594, Jun. 1987.

[8] R. Tandra and A. Sahai, "SNR walls for signal detection," *IEEE J. Sel. Topics Signal Process.*, vol. 2, no. 1, pp. 4–17, Feb. 2008.

[9] A. Surampudi and K. Kalimuthu, "An adaptive decision threshold scheme for the matched filter method of spectrum sensing in cognitive radio using artificial neural networks," in *Proc. 1st India Int. Conf. Inf. Process. (IICIP)*, New Delhi, India, Aug. 2016, pp. 1–5.

[10] M. Yang, Y. Li, X. Liu, and W. Tang, "Cyclostationary feature detection based spectrum sensing algorithm under complicated electromagnetic environment in cognitive radio networks," *China Commun.*, vol. 12, no. 9, pp. 35–44, Sep. 2015.

[11] Y. Zhang, S. Zhang, Y. Wang, J. Zhuang, and P. Wan, "Riemannian mean shift-based data fusion scheme for multi-antenna cooperative spectrum sensing," *IEEE Trans. Cogn. Commun. Netw.*, vol. 8, no. 1, pp. 47–56, Mar. 2022.

[12] Y. Zeng, Y.-C. Liang, A. T. Hoang, and R. Zhang, "A review on spectrum sensing for cognitive radio: Challenges and solutions," *EURASIP J. Adv. Signal Process.*, vol. 2010, Jan. 2010, Art. no. 381465. [Online]. Available: https://doi.org/10.1155/2010/381465

[13] A. Eslami and G. K. Kurt, "Proposal and analysis of consecutive results maximum to minimum eigenvalue spectrum sensing algorithm," in *Proc. 40th Int. Conf. Telecommun. Signal Process. (TSP)*, Barcelona, Spain, Oct. 2017, pp. 165–169.

[14] Z.-L. Wang, X.-O. Song, and X.-R. Wang, "Spectrum sensing detection algorithm based on eigenvalue variance," in *Proc. IEEE 8th Joint Int. Inf. Technol. Artif. Intell. Conf. (ITAIC)*, Chongqing, China, May 2019, pp. 1656–1659.

[15] Y. Zeng and Y. Liang, "Spectrum-sensing algorithms for cognitive radio based on statistical covariances," *IEEE Trans. Veh. Technol.*, vol. 58, no. 4, pp. 1804–1815, May 2009.

[16] C. Gattoua, O. Chakkor, and F. Aytouna, "An overview of cooperative spectrum sensing based on machine learning techniques," in *Proc. IEEE 2nd Int. Conf. Electron. Control Optim. Comput. Sci. (ICECOCS)*, Kenitra, Morocco, Dec. 2020, pp. 1–8.

[17] K. M. Thilina, K. W. Choi, N. Saquib, and E. Hossain, "Machine learning techniques for cooperative spectrum sensing in cognitive radio networks," *IEEE J. Sel. Areas Commun.*, vol. 31, no. 11, pp. 2209–2221, Nov. 2013.

Authorized licensed use limited to: HANGZHOU DIANZI UNIVERSITY. Downloaded on October 18,2023 at 00:43:50 UTC from IEEE Xplore. Restrictions apply.

[18] J. Bao, B. Lu, B. Jiang, J. Wu, and C. Liu, "Cooperative blind spectrum detection with doolittle decomposition and PCA-SVM classification in hybrid GEO-LEO satellite constellation networks," *IEEE Trans. Aerosp. Electron. Syst.*, vol. 57, no. 5, pp. 3209–3220, Oct. 2021.
[19] C. Liu, J. Wang, X. Liu, and Y.-C. Liang, "Deep CM-CNN for spectrum sensing in cognitive radio," *IEEE J. Sel. Areas Commun.*, vol. 37, no. 10, pp. 2306–2321, Oct. 2019.
[20] W. Lee, M. Kim, and D. Cho, "Deep cooperative sensing: Cooperative spectrum sensing based on convolutional neural networks," *IEEE Trans. Veh. Technol.*, vol. 68, no. 3, pp. 3005–3009, Mar. 2019.
[21] D. He, Y. Lin, C. He, and L. Jiang, "A novel spectrum-sensing technique in cognitive radio based on stochastic resonance," *IEEE Trans. Veh. Technol.*, vol. 59, no. 4, pp. 1680–1688, May 2010.
[22] K. Zheng, H. Li, S. Djouadi, and J. Wang, "Spectrum sensing in low SNR regime via stochastic resonance," in *Proc. Conf. Inf. Sci. Syst. (CISS)*, Princeton, NJ, USA, Mar. 2010, pp. 1–5.
[23] R. Benzi, A. Sutera, and A. Vulpiani, "The mechanism of stochastic resonance," *J. Phys. A Math. Gen.*, vol. 14, no. 11, pp. 453–457, Nov. 1981.
[24] G.-F. Wang, H.-R. Zhang, F.-Q. Zhang, J.-C. Ye, and L. Wei, "Scale transformation stochastic resonance for a weak signal detection," in *Proc. 11th World Congr. Mech. Mach. Sci.*, Apr. 2004, pp. 1–9.
[25] Z. Qiao, Y. Lei, J. Lin, and F. Jia, "An adaptive unsaturated bistable stochastic resonance method and its application in mechanical fault diagnosis," *Mech. Syst. Signal Process.*, vol. 84, pp. 731–746, Feb. 2017.
[26] H. B. Zhang, Q. He, S. Lu, and F. Kong, "Stochastic resonance with a joint Woods–Saxon and Gaussian potential for bearing fault diagnosis," *Math. Probl. Eng.*, vol. 2014, Jun. 2014, Art. no. 315901. [Online]. Available: https://doi.org/10.1155/2014/315901
[27] S. Jiao, S. Lei, W. Jiang, Q. Zhang, and W. Huang, "A novel type of stochastic resonance potential well model and its application," *IEEE Access*, vol. 7, pp. 160191–160202, 2019.
[28] U. R. Umar and A. U. H. Sheikh, "A comparative study of spectrum awareness techniques for cognitive radio oriented wireless network," *Phys. Commun.*, vol. 9, pp. 148–170, Dec. 2013.
[29] W. Zhang, R. Mallik, and K. Letaief, "Optimization of cooperative spectrum sensing with energy detection in cognitive radio networks," *IEEE Trans. Wireless Commun.*, vol. 8, no. 12, pp. 5761–5766, Dec. 2009.
[30] D. Romero and R. López-Valcarce, "Spectrum sensing for wireless microphone signals using multiple antennas," *IEEE Trans. Veh. Technol.*, vol. 63, no. 9, pp. 4395–4407, Nov. 2014.
[31] L. Gammaitoni, P. Hänggi, P. Jung, and F. Marchesoni, "Stochastic resonance," *Rev. Mod. Phys.*, vol. 70, no. 1, pp. 223–287, Jan. 2008.
[32] B. McNamara and K. Wiesenfield, "Theory of stochastic resonance," *Phys. Rev. A*, vol. 39, no. 9, pp. 4854–4869, Jan. 1989.
[33] D. R. Pauluzzi and N. C. Beaulieu, "A comparison of SNR estimation techniques for the AWGN channel," *IEEE Trans. Commun.*, vol. 48, no. 10, pp. 1681–1691, Oct. 2000.
[34] P. Leng et al., "Logistic regression based on artificial fish swarm algorithm with T-Distribution parameters," in *Proc. IEEE 9th Joint Int. Inf. Technol. Artif. Intell. Conf. (ITAIC)*, vol. 9. Chongqing, China, Dec. 2020, pp. 1912–1915.
[35] M. Z. Shakir, A. Rao, and M. Alouini, "Collaborative spectrum sensing based on the ratio between largest eigenvalue and geometric mean of eigenvalues," in *Proc. IEEE GLOBECOM Workshops (GCWkshps)*, Dec. 2011, pp. 913–917.

Bin Jiang received the B.S. and M.S. degrees in communication and electronic system from the School of Communication Engineering, Hangzhou Dianzi University, Hangzhou, China, in 1999 and 2004, respectively, where he is currently pursuing the Ph.D. degree in electronic science and technology with the School of Electronics and Information.

He is currently a Senior Experimentalist with the School of Communication Engineering, Hangzhou Dianzi University. His main research interests include wireless communications, signal processing, and information theory and coding.

Yuefei Cao received the B.S. degree in communication engineering from the School of Communication Engineering, Hangzhou Dianzi University, Hangzhou, China, in 2020, where he is currently pursuing the master's degree in information and communication engineering with the School of Communication Engineering.

His research interests include wireless communications and cognitive radio.

Jianrong Bao (Senior Member, IEEE) received the B.S. degree in polymeric materials and engineering and the M.S. degree in communication and information system from the Zhejiang University of Technology, Hangzhou, China, in 2000 and 2004, respectively, and the Ph.D. degree in information and communication engineering from the Department of Electronic Engineering, Tsinghua University, Beijing, China, in 2009.

He is currently a Professor with the School of Communication Engineering, Hangzhou Dianzi University, Hangzhou, China. His main research interests include wireless communications, cognitive radio, and information theory and coding.

Chao Liu received the B.S. and Ph.D. degrees in information and communication engineering from the School of Electronic Information and Communications, Huazhong University of Science and Technology, Wuhan, China, in 2000 and 2005, respectively.

He is currently an Associate Professor with the School of Communication Engineering, Hangzhou Dianzi University, Hangzhou, China. His research interests include modern wireless communication and coding, and MIMO multi-user detection.

Xianghong Tang received the B.S. degree in physics from Southwest Normal University, Chongqing, China, in 1985, the M.S. degree in physics from Sichuan University, Chengdu, China, in 1988, and the Ph.D. degree in EE from the University of Electronic Science and Technology, Chengdu, in 1997.

He is a Professor with the School of Communication Engineering, Hangzhou Dianzi University, Hangzhou, China. His research interests include multimedia signal processing, information theory, and source/channel coding.

Authorized licensed use limited to: HANGZHOU DIANZI UNIVERSITY. Downloaded on October 18,2023 at 00:43:50 UTC from IEEE Xplore. Restrictions apply.